

Water Resources Research



RESEARCH ARTICLE

10.1029/2022WR033026

Key Points:

- Satellite remote sensing can improve the representation of ungauged reservoirs and streamflow simulations in hydrologic models
- A reservoir operation scheme for ungauged reservoirs is extended and tailored to the use of remotely sensed reservoir operation data
- Reservoir operation schemes with storage-based model structures can be more reliable in reservoir simulations under a changing flow regime

Supporting Information:

Supporting Information may be found in the online version of this article.

Correspondence to:

J. Wei and Z. Yu,
jianhui.wei@kit.edu;
zyu@hhu.edu.cn

Citation:

Dong, N., Yang, M., Wei, J., Arnault, J., Laux, P., Xu, S., et al. (2023). Toward improved parameterizations of reservoir operation in ungauged basins: A synergistic framework coupling satellite remote sensing, hydrologic modeling, and conceptual operation schemes. *Water Resources Research*, 59, e2022WR033026. <https://doi.org/10.1029/2022WR033026>

Received 13 JUN 2022
Accepted 19 FEB 2023








Author Contributions:

Conceptualization: Ningpeng Dong
Formal analysis: Ningpeng Dong
Funding acquisition: Ningpeng Dong, Jianhui Wei
Methodology: Ningpeng Dong
Project Administration: Ningpeng Dong
Writing – original draft: Ningpeng Dong

© 2023. The Authors.

This is an open access article under the terms of the [Creative Commons Attribution-NonCommercial-NoDerivs License](https://creativecommons.org/licenses/by/4.0/), which permits use and distribution in any medium, provided the original work is properly cited, the use is non-commercial and no modifications or adaptations are made.

Toward Improved Parameterizations of Reservoir Operation in Ungauged Basins: A Synergistic Framework Coupling Satellite Remote Sensing, Hydrologic Modeling, and Conceptual Operation Schemes

Ningpeng Dong^{1,2,3,4} , Mingxiang Yang^{1,4}, Jianhui Wei⁵ , Joël Arnault⁵ , Patrick Laux^{5,6} , Shiqin Xu^{7,8} , Hao Wang¹, Zhongbo Yu² , and Harald Kunstmann^{5,6} 

¹State Key Laboratory of Simulation and Regulation of Water Cycle in River Basin, China Institute of Water Resources and Hydropower Research, Beijing, China, ²State Key Laboratory of Hydrology-Water Resources and Hydraulic Engineering, Hohai University, Nanjing, China, ³Key Laboratory of Flood and Drought Disaster Defense, Ministry of Water Resources, Nanjing, China, ⁴Cooperative Innovation Center for Water Safety & Hydro Science, Nanjing, China, ⁵Institute of Meteorology and Climate Research (IMK-IFU), Karlsruhe Institute of Technology, Campus Alpin, Garmisch-Partenkirchen, Germany, ⁶Institute of Geography, University of Augsburg, Augsburg, Germany, ⁷College of Geography and Environmental Science, Northwest Normal University, Lanzhou, China, ⁸Key Laboratory of Resource Environment and Sustainable Development of Oasis, Beijing, China

Abstract Assessments of water and energy security over historical and future periods require hydrologic models that can accurately simulate reservoir operations. However, scarce reservoir operation data limits the accuracy of current reservoir representations in simulating reservoir behaviors. Furthermore, the reliability of these representations under changing inflow regimes remains unclear, which makes their application for long future planning horizons questionable. To this end, we propose a synergistic framework to predict the release, storage, and hydropower production of ungauged reservoirs (i.e., reservoirs without in-situ inflow, release, storage, and operating rules) by combining remotely sensed reservoir operating patterns and model-simulated reservoir inflow with conceptual reservoir operation schemes within a land surface-hydrologic model. A previously developed reservoir operation scheme is extended with a storage anomaly based calibration approach to accommodate the relatively short time series and large time intervals of remotely sensed data. By setting up controlled experiments in the Yalong River Basin in China, we show that remote sensing can improve the parameter estimation and simulations of ungauged reservoirs for all selected reservoir operation schemes, thereby improving the downstream flood and streamflow simulations. However, most of these schemes show degraded accuracies of reservoir operation simulations under a changing inflow regime, which could lead to unreliable assessments of future water resources and hydropower production. In comparison, our newly extended reservoir operation scheme can be more adaptable to flow regime variations. Our study provides a practical framework for reservoir impact assessments and predictions with the ongoing satellite altimetry projects such as Surface Water and Ocean Topography.

1. Introduction

Increasing water and energy demands have been posing large challenges for sustainable social-economic development given current global population growth and warming climate (Liu et al., 2017; O'Neill et al., 2017). The United Nations predicts that, by 2030, over 20% and 8% of the global population are expected to be living in regions with absolute scarcity of water and electricity, respectively (Gain et al., 2016). The construction of reservoirs is one of the most practical strategies to alleviate the water and energy shortage (J. Wang et al., 2022; Xu et al., 2023; W. Zhong et al., 2020). The global total water storage capacity of reservoirs reach up to around three times the annual average water storage in river channels (Hanasaki et al., 2006), and the global hydropower production in 2016 is approximately three times higher than it was in 1973 (Wan et al., 2021).

To assess the impact of planned and existing reservoirs on energy systems and their alterations to hydrologic regimes, hydrologic models have been developed with varying degrees of complexity of reservoir representations (Arheimer et al., 2017; Giuliani et al., 2016; Grill et al., 2014; Hoang et al., 2019; Lu et al., 2018; Wan et al., 2021). These include the incorporation of reservoir operation at regional scales (Fleischmann et al., 2021; Turner et al., 2020; Y. Wang et al., 2019; Wei et al., 2021; G. Zhao et al., 2016), national scales

Writing – review & editing: Mingxiang Yang, Jianhui Wei, Joël Arnault, Patrick Laux, Shiqin Xu, Hao Wang, Zhongbo Yu, Harald Kunstmann

(Ehsani et al., 2017), and global scales (Hanasaki et al., 2018; Veldkamp et al., 2018; Wada et al., 2016; Wisser et al., 2010). Currently, this is often achieved by coupling reservoir operation schemes that can generally be divided into conceptual ones and data-driven ones. Conceptual reservoir operation schemes estimate the release of reservoirs by establishing empirical functions between release, storage, inflow, and/or water demand, which include simpler ones that are designed for large-scale applications with minimum data requirements (Hanasaki et al., 2008; Shin et al., 2019; Solander et al., 2016) and more sophisticated ones that require long-term operation data for parameter calibration (Wu & Chen, 2012; G. Zhao et al., 2016). Data-driven models, on the other hand, deduce reservoir releases by training machine learning regression algorithms on extensive reservoir operation data (Dong et al., 2023; Yang et al., 2019). Both models have advantages and disadvantages. When fed with a sufficiently large amount of data, data-driven models often outperform conceptual models, yet their black-box nature often hinders modelers from understanding the mechanism of reservoir operation and may yield unreliable results in case of extrapolation beyond training data (Yassin et al., 2019).

Despite the progress in representing reservoirs in hydrologic simulations, uncertainties still exist in modeled reservoir releases and storages, especially for reservoirs with no in-situ operation data (inflow, release, storage, etc.) (hereinafter “ ungauged reservoirs”) (Dang et al., 2020; Yassin et al., 2019). Although a variety of reservoir operation schemes have been developed to reproduce observed reservoir storages and releases, these schemes often introduce structures or parameters that need to be estimated from historic reservoir operation records or inferred from detailed operation rules for individual reservoirs (Hoang et al., 2019; Wisser et al., 2010; Zajac et al., 2017). However, these data are often unavailable to researchers especially when there is limited stakeholder engagement. This leads to a decreased accuracy of reservoir behavior simulations at regional and larger scales (Ehsani et al., 2016). Recently, Dong et al. (2022) proposed a calibration-free conceptual operation scheme for ungauged reservoirs in the CLHMS model to simulate the reservoir operation of over 3,000 reservoirs in China. Despite this advance, the performance of these reservoir operation schemes generally falls short of the accuracy requirements for reservoir impact assessment at finer scales.

With recent developments in satellite altimetry, it has been possible to derive the water level of reservoirs and lakes remotely, providing a promising solution to overcome the scarcity of reservoir operation data (Avisse et al., 2017; Busker et al., 2019; Crétaux et al., 2015; Fan et al., 2020; Gao et al., 2012; Huang et al., 2020; Li et al., 2019). Since the launch of altimetry satellites, such as Jason, Sentinel, and the Ice, Cloud and land Elevation Satellite (ICESat), many studies have combined satellite-derived water levels with remotely sensed reservoir surface areas to derive estimates of reservoir water storage (Chen, Song, Luo, et al., 2022; Cooley et al., 2021; Gao, 2015; Shen et al., 2022) and infer reservoir operation policies (Bonnema & Hossain, 2017, 2019). Several studies have also combined the satellite-derived reservoir storage variation with the conservation of mass principle to determine the reservoir releases for downstream hydrologic simulations (Vu et al., 2022; Yoon & Beighley, 2015; Yoon et al., 2015; R. Zhong et al., 2020). In most of these cases, remote sensing is used to provide the storage variation term in the water balance equation, which does not involve the parameterizations of reservoir operation as noted earlier, making it less applicable for hydrologic simulations and forecasts in the future. Having said that, the potential of this readily available information for improving the parameter estimation of current reservoir operation schemes and enhancing the accuracy of hydrologic predictions in ungauged, regulated basins has been less investigated (Du et al., 2022).

In addition to challenges with simulating the behavior of reservoirs without operation data, the applicability of reservoir parameters estimated during historical periods may decrease under different future conditions. This brings into question the accuracy of the simulated reservoir operation over a long-term (e.g., multi-year) period. Taking parameters of hydrologic models as an example, Dang et al. (2020) found that the optimal parameter values of the VIC model in the Mekong River Basin varied over time with the ongoing construction of water infrastructures along the mainstream. Similarly, Ruijsch et al. (2021) revealed that optimal parameter values of the PCR-GLOBWB model for the Rhine and Meuse basin in Europe vary with the changes in regional climate, land use, and river structure, highlighting the need to assess model applicability in a changing environment. To our knowledge, however, such an assessment has been missing in reservoir modeling, and there exists a gap in knowledge about the reliability of the employed reservoir operation scheme tuned on historic data in simulating future reservoir operations under a changing streamflow regime.

To enhance the understanding of predictive uncertainties in reservoir representations in hydrologic models, our study aims to address the following two research questions:

1. How can satellite remote sensing be leveraged to improve the reservoir operation parameterizations and the simulation accuracy of ungauged reservoirs?
2. How can reservoir parameterizations derived from past experiences predict reservoir behaviors more accurately under future changes in inflow?

To answer these questions, we propose a synergistic framework that combines remotely sensed reservoir operation data and simulated reservoir inflow with several widely used conceptual reservoir operation schemes within a coupled land surface-hydrologic model. Among the selected reservoir schemes, a calibration-free operation scheme for ungauged reservoirs developed in our previous study (Dong et al., 2022) is further extended with a storage anomaly-based calibration approach that is tailored to the use of remotely sensed data. We select the Yalong River Basin (YRB) in China with two large hydropower reservoirs, namely Jinping I and Ertan, as our target region to evaluate the applicability of our framework. The YRB is selected because it is a major water source of the Yangtze River and serves as the third largest hydropower base of the country in terms of installed capacity, with several large-sized hydropower reservoirs already in operation and a dozen more under construction and or in planning stages (Gu et al., 2018). An accurate depiction of the water-energy nexus of the basin is beneficial to understand the evolution of regional water and energy security and sustainability. Moreover, it could also provide implications for similar basins in different regions worldwide, especially ones with a paucity of reservoir operation data and/or available operating rules.

2. Study Area

The YRB is located in the upper Yangtze River Basin, with an area of 1.36×10^5 km² (Figure 1). The basin lies on the eastern edge of the Tibetan Plateau and is characterized by subtropical highland climate, rugged terrain, and sparse population. The average annual precipitation of the basin is approximately 800 mm. Nearly 75% occurs between June and October, thus partitioning a year into the wet and dry seasons. The Ertan station, located immediately upstream of the Ertan Reservoir, is the downstream-most hydrologic station of the basin.

Since early 2010s, there have been two large hydropower reservoirs constructed in the mainstream with a sufficient capacity to regulate the streamflow, namely Ertan and Jinping I. The Ertan Reservoir started operation in 1998 and has a capacity of 6.1×10^9 m³, accounting for around 13% of the mean annual inflow. The Jinping I Reservoir was put into normal operation in mid-2014 and had a capacity of 8.0×10^9 m³, accounting for around 20% of its mean annual inflow. These two reservoirs had independent operation policies during the study period of 2010–2018.

3. Data and Methods

Our proposed framework assumes the in-situ inflow, release, storage, and operation rules are not available for the Ertan Reservoir and Jinping I Reservoir during the modeling processes. A coupled land surface-hydrologic model (CLHMS) is employed as the underlying model for simulations of reservoir operation and streamflow. The Jason-2/3 satellite altimetry is used to extract the historic water level data of the two reservoirs, which are then combined with remotely sensed reservoir water area and model-simulated inflow to reconstruct their surface area-water level relationship along with their storage and release data and average operating patterns. These new data provide the initial conditions, calibration data, and/or target storages and releases for four conceptual reservoir operation schemes. Among these schemes, our previously developed reservoir operation scheme is particularly extended and tailored to the use of remotely sensed data. All these schemes are then separately two-way coupled to the CLHMS model for improved simulations of ungauged reservoirs. The applicability of our presented synergistic framework is finally investigated under the changing flow regime of the YRB in terms of the release, storage, and hydropower simulations of both reservoirs and the streamflow simulations of the CLHMS model. A general workflow of this study is presented in Figure 2.

3.1. Data Sources

Data collected in this study include input data for the hydrologic model, in-situ streamflow data, satellite altimetry data, reservoir attributes, and in-situ reservoir operation data etc.

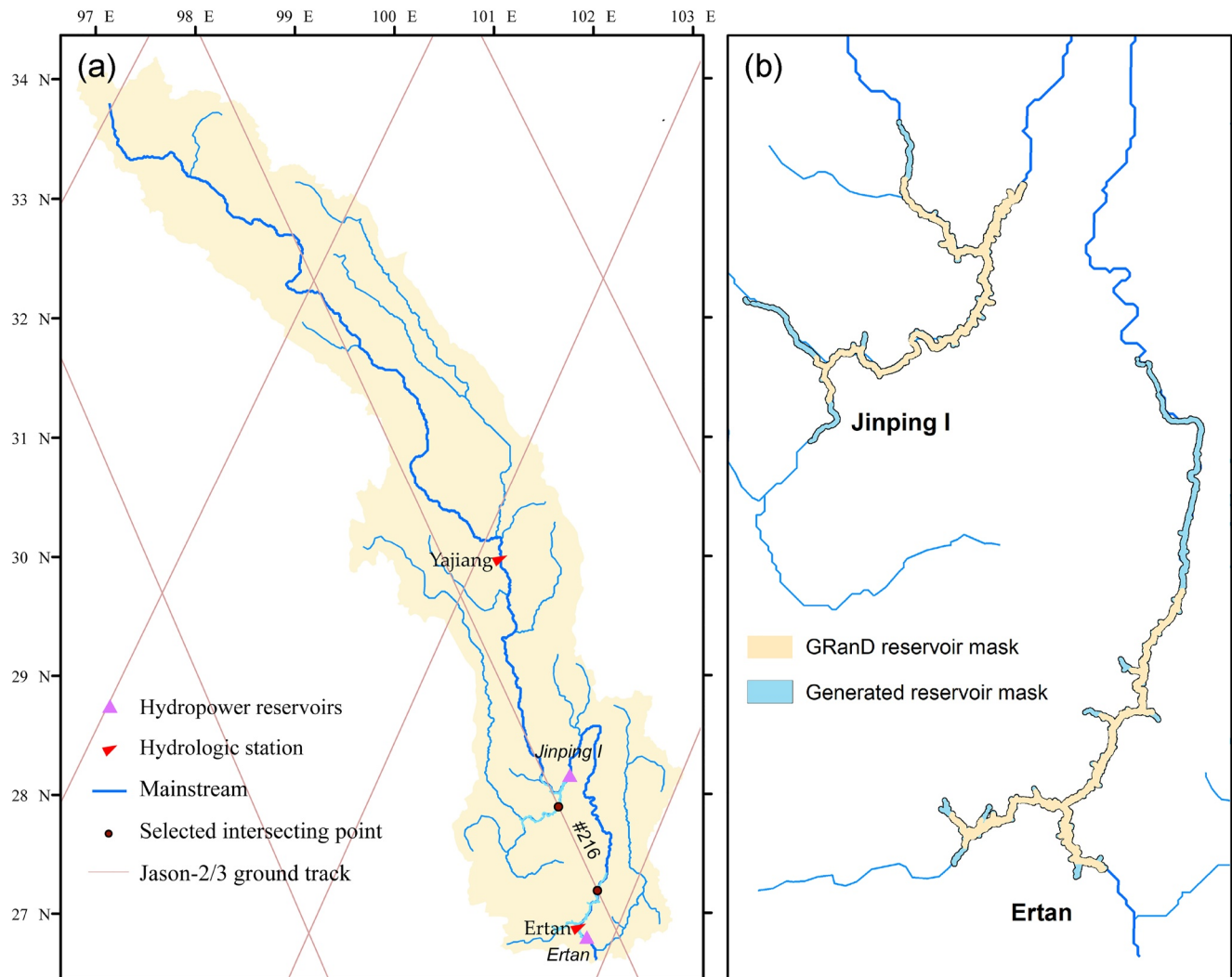


Figure 1. (a) The Yalong River Basin, where the Jason-2/3 ground track #216 intersects Jinping I and Ertan Reservoir (Section 3.1); and (b) the Jinping I Reservoir and Ertan Reservoir with GRanD reservoir masks and our generated reservoir masks (Section 3.4).

3.1.1. Input Data for the Hydrologic Model

To drive the CLHMS model for simulation of reservoirs and associated streamflow and hydropower production, meteorological forcing, soil texture, and geology data are required as model inputs. In this study, the meteorological data consist of the CN05.1 data set for precipitation (Wu & Gao, 2013) and the NCEP/NCAR reanalysis data for air temperature, wind speed, solar radiation, air pressure, and specific humidity (Kalnay et al., 1996). The CN05.1 data set published by China Meteorological Administration is a $0.25^\circ \times 0.25^\circ$ gridded precipitation data set interpolated from the observed precipitation of $\sim 2,400$ rain gauges nationwide. The meteorological forcing is bilinearly interpolated to the model resolution. The soil texture and properties are collected from the Harmonized World Soil Database (HWSD) (Nachtergaele et al., 2010). The HydroSHEDs DEM (Lehner et al., 2011) is used as surface elevation input of the hydrologic model, and the land use is obtained from the AVHRR (Advanced Very High-Resolution Radiometer) (Loveland et al., 2000).

3.1.2. In Situ Streamflow Data

The in-situ daily streamflow of the Yajiang station for the period of 2006–2011 and the Ertan station for the period of 2001–2018 is collected in this study to calibrate and validate the CLHMS model (Figure 1). Note that Jinping I operated around 2014.

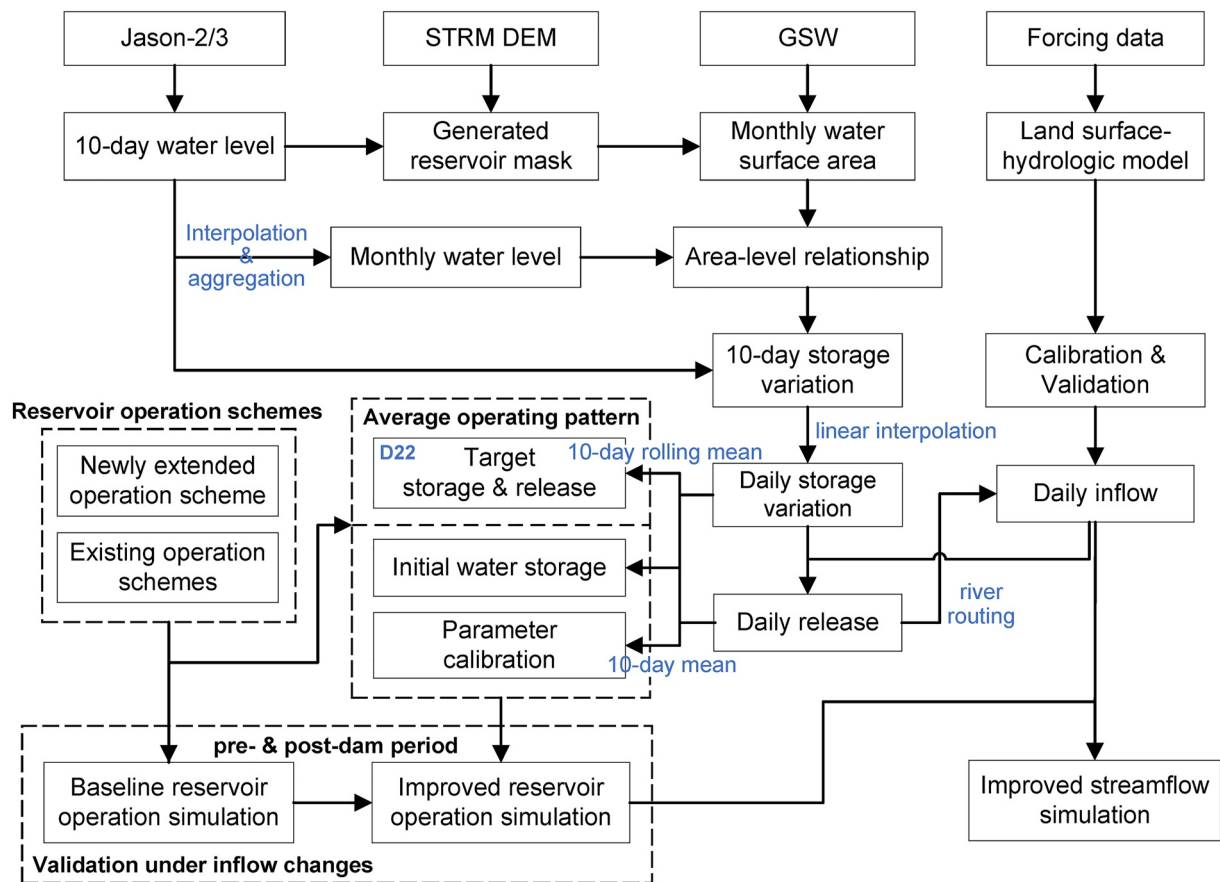


Figure 2. A general workflow of this study.

3.1.3. Satellite Altimetry Data

Jason-2/3 satellite altimetry data provided by the Centre National d'Etudes Spatiales (CNES) (AVISO CNES Data Center, 2018) are used in this study to derive the historic water level of Ertan Reservoir for 2010–2018 and that of Jinping I Reservoir for 2015–2018. The Jason-2/3 is selected because it has a relatively short revisit frequency (10 days) and it intersects these two reservoirs along its track #216.

3.1.4. Surface Water Extent

The JRC global surface water (GSW) data set is employed to calculate the reservoir water area, which provides rasterized monthly water extent at a spatial resolution of ~30 m at global scales (JRC, 2016; Pekel et al., 2016). The Global Reservoir Surface Area Dataset (GRSAD) provides the values of the global monthly reservoir water area (Gao & Zhao, 2019) and is also collected for comparison with the reservoir water area derived in our study. In GRSAD, the reservoir area values are derived by masking GSW raster data with GRanD reservoir polygons.

3.1.5. Digital Elevation Data

The SRTM DEM is used to generate the reservoir boundary mask for reservoir water area calculation, which was generated by an interferometric synthetic aperture radar (InSAR) system on board the Space Shuttle Endeavor in February 2000 and provides the surface elevation data at a spatial resolution of 30 m.

3.1.6. Reservoir Attributes

The location, dead storage, conservation storage, and capacity of the Jinping Reservoir and the Ertan Reservoir are collected from the Changjiang Water Resources Commission (CWRC). Static reservoir attributes are generally widely shared in China, which can also be retrieved from the literature.

3.1.7. In Situ Reservoir Operation Records for Validation

The historic in-situ release, storage, and hydropower output of the Ertan Reservoir and the Jinping I Reservoir are collected to evaluate the reservoir storage and release reconstructed from remote sensing (Section 3.5), and the reservoir operation simulations using conceptual reservoir operation schemes (Section 3.6). These data are collected from CWRC and can be downloaded from Dong (2022).

3.2. The Coupled Land Surface and Hydrologic Model System

In this study, the CLHMS, that is, a fully coupled system of the land surface scheme of GENESIS (LSX) and the physically based Hydrological Model System (HMS) (Yu et al., 1999, 2006), is employed to simulate the reservoir-regulated hydrologic regime of the YRB at a spatial resolution of 5 km. The LSX vertically solves the water and energy balance in the land and calculates the runoff, infiltration, evapotranspiration, and other hydrologic components over each grid cell, while the HMS solves the river runoff routing and soil moisture transport on a grid basis with the diffusion wave equation and steady-state Richards equation, respectively (Wagner et al., 2016). The model is also coupled with a 2-D groundwater routing model, which can explicitly solve groundwater hydrodynamics (Yu et al., 2006). The model is deployed in the high-performance cluster in the State Key Laboratory of Simulation and Regulation of Water Cycle in River Basin of China, which allows ~100 parallel model runs.

3.3. Reconstructing Reservoir Water Level From Satellite Altimetry

In this study, the historic water level of two mainstream reservoirs, namely Jinping I and Ertan Reservoir, is reconstructed from the Geophysical Data Record (GDR) of the Jason-2/3 satellite altimetry from 2010 to 2018 and from 2015 to 2018, respectively, at a revisiting frequency of 10 days. For each of the satellite footprints within the maximum surface water extent of reservoirs, the water level with respect to the reference geoid (i.e., EGM96 in this study), H , is derived following Huang et al. (2018, 2020):

$$H = H_{alt} - H_{ran} - H_{cor} \quad (1)$$

with

$$H_{cor} = wtc + dtc + ic + setc + ptc \quad (2)$$

where H_{alt} is the altitude of the satellite with respect to the geoid, H_{ran} is the distance between the reservoir water surface and the satellite; H_{cor} is the correction term, which consists of the wet tropospheric (wtc), dry tropospheric (dtc), ionospheric (ic), solid Earth tide ($setc$), and polar tide corrections (ptc), respectively. These data are provided in the GDR files.

For each revisiting cycle, there are many available satellite footprints and corresponding water level data within the reservoir geospatial boundary provided by the Global Reservoir and Dam (GRanD) database (Lehner et al., 2011). However, many of them are subject to land contamination and other sources of noise in satellite signals. To improve the quality of water level retrieval, we exclude any data beyond three times the standard deviation of the water level, and then select the median of remaining water level data as the resulting water level. Valid water level data are not guaranteed for all of the revisiting cycles due to the data noise. Invalid data are discarded and then filled by linear interpolation between the previous and next 10-day cycles. In all, invalid cycles account for 5%–7% of the total cycles. Given that 70%–80% of these invalid cycles occur in the dry season where the water level often changes in a steady manner, the linear interpolation is unlikely to have induced large errors.

3.4. Estimating Water Area for Channel-Type Reservoirs With Improved Boundary Masks

By combining the altimetric water level with the surface water area from remote sensing images, the reservoir water storage variations can be approximated (Busker et al., 2019; Gao et al., 2012). To derive the surface water area, a rigorous reservoir boundary mask is required to identify the maximum extent to which the reservoir water area is to be extracted. Here, GRanD and other existing reservoir databases may not be applicable for this purpose because their reservoir masks are derived by visually identifying the maximum water extent from remote sensing images. While this often works well for lake-type reservoirs, the identified maximum water extent and hence

the mask in some cases can be smaller for channel-type reservoirs, because narrow reservoir sections could be mistakenly identified as river channels due to the lack of an easily visible boundary between the river channel and the upstream end of the reservoir pools.

In light of this issue, one solution is to compare the maximum water area of remote sensing images before and after the construction of reservoirs to derive the reservoir water extent. However, due to the serious cloud contaminations during the wet season and the limited coverage of optical remote sensing satellites before 2000 (Pekel et al., 2016), this solution is inapplicable to the majority of reservoirs in China. Therefore, we employ the SRTM DEM data and altimetric reservoir water level to derive the reservoir boundary. The reservoir boundary extent is identified as the area where the STRM DEM surface elevation is no larger than the highest altimetric reservoir water level determined in Section 3.3. A mask is then generated by buffering 500 m outward from this DEM-based reservoir boundary. Note that this mask does not necessarily represent the maximum extent of that reservoir. However, it is considered to encompass all water pixels that can be used to establish the area-elevation relationship with any of the altimetric water levels.

To derive the reservoir water area within the generated reservoir mask, the JRC (GSW data set is employed, which provides the monthly water extent at a spatial resolution of ~30 m at global scales (Pekel et al., 2016). Due to the contamination of clouds, snow, ice, and terrain shadows, a large number of no-data pixels exist in the GSW data set, which could lead to the underestimation of the surface water area. To this end, we calculate the no-data ratio by dividing the number of no-data pixels in each month by the total number of pixels within the generated reservoir mask. If the no-data ratio is larger than 5%, the GSW data for this month is excluded from the analysis. The monthly reservoir water area is then calculated by multiplying the number of water pixels by the spatial resolution of a pixel.

To demonstrate the improvement of our derived reservoir mask and hence the water area against current products, the monthly water area of the two reservoirs is first collected from the Global Reservoir Surface Area Dataset (GRSAD) (Gao & Zhao, 2019), which employs the GRanD reservoir mask to derive the global monthly reservoir water area values. We then reconstruct the reservoir water storage with (a) the derived GSW monthly water area (i.e., based on our generated DEM-based reservoir mask) and (b) the GRSAD monthly water area (i.e., based on the GRanD reservoir mask) in the following section for comparison, respectively.

3.5. Deriving Reservoir Storages, Releases, and Average Operating Patterns

The 10-day altimetric water level in Section 3.3 is firstly linearly interpolated to produce daily values and then averaged on a monthly basis to match the monthly water area in Section 3.4 (Busker et al., 2019). The monthly water level and water area are then used to establish an empirical water area-level relationship for reservoirs, that is,

$$A = f(h) = a \cdot h + b \quad (3)$$

where h is the monthly reservoir water level; A is the monthly reservoir water area; a and b are the slope and intercept parameters derived by least square regression. Linear area-elevation functions have been widely adopted in previous studies, for example, Gao et al. (2012), Eldardiry & Hossain, 2019, Chen, Song, Zhan, et al. (2022). While functions of higher order can also be employed, there can be a risk of overfitting due to the limited set of remotely sensed area-elevation data pairs in our study, which could cause large errors beyond the range of the available data. Another common approach to establishing the area-level relationship is to calculate the area encircled by each 1-m elevation of the DEM. We did not opt for this approach because Ertan had already been filled at the time STRM was launched, and most of the terrain information was not available.

The 10-day altimetric water level is then used to reconstruct the 10-day historic reservoir storage variation with the simplified storage update equation of Equation 4 (Gao et al., 2015), that is, a single variable function of water level with the area-level relationship (Equation 3):

$$\Delta V = \Delta h \cdot \bar{A} = \Delta h \cdot (a \cdot \bar{h} + b) \quad (4)$$

where ΔV and Δh are the absolute variation of the reservoir storage and altimetric water level during the 10-day intervals; \bar{h} is the average water level at the beginning of two continuous 10-day interval. To calculate

the absolute reservoir storage at each time step, a set of initial values of h and V are required to complement Equation 4. Here, we assume that the multi-year maximum monthly value of the water level during the dry season, h_{maxd} , corresponds to the conservation pool level in the dry season and its corresponding storage V_{cd} (see Figure S4 in Supporting Information S1 for illustrations), providing Equation 4 with a known data point (h_{maxd}, V_{cd}) and hence a unique solution. It is a reasonable assumption because both reservoirs are within-year reservoirs that are designed to return to the conservation level at the dry season in most of the years. For some of the over-year reservoirs with very large capacities, on the other hand, it may take longer for them to return to the conservation level than within-year reservoirs, and in this case longer remote sensing records are desirable.

With the reservoir storage computed, we next use CLHMS as the underlying model to reconstruct the inflow and release of the Jinping I Reservoir and the Ertan Reservoir. To achieve an accurate streamflow simulation across the YRB and hence the inflow of reservoirs, we first calibrate the model to the daily streamflow at the Yajiang station and the Ertan station, with results provided in Section 4.1. Then, the daily inflow of the Jinping I Reservoir is simulated by the CLHMS model and combined with the altimetry-based reservoir storage to reconstruct its historic release at a daily scale:

$$\bar{Q} = \bar{I} + \bar{P} - \bar{E} - \frac{\Delta V}{\Delta t} \quad (5)$$

where \bar{I} , \bar{Q} , \bar{P} , and \bar{E} are the daily averaged inflow, release, precipitation, and evaporation of the reservoir, respectively. ΔV is the daily storage variation that is linearly interpolated from the reconstructed storage variation at the 10-day interval, and Δt is the time step (daily). The reservoir evaporation rate is calculated based on Penman's equation (McMahon et al., 2013; Penman, 1948). We closely follow Zhao and Gao (2019) and Tian et al. (2021) for detailed calculation procedures, which are given in Text S1 in Supporting Information S1. Infiltration and recharge are not considered in the reservoir water balance because both reservoirs lie in a rocky valley covered mostly by basalt rock that has a rather low permeability, which prevents considerable groundwater-reservoir water exchange (CECL, 2003).

Given that the Ertan Reservoir is downstream of the Jinping I Reservoir, the simulated streamflow at Jinping I is substituted by the reconstructed release of Jinping I, which is then routed downstream to reconstruct the daily inflow of Ertan in the CLHMS model. The above reservoir water balance calculation is then repeated for the Ertan Reservoir to reconstruct its historic release at a daily scale.

Averaging the reconstructed reservoir storage and release at different times of the year allows us to derive the average reservoir operating patterns that are represented by target storages and target releases. Target storages refer to the average storage levels that a reservoir normally reaches at different times of the year, corresponding to the average reservoir operation rule curve as illustrated in Figure S4 in Supporting Information S1. Target releases refer to the average amount of water that a reservoir normally releases at different times of the year, which implicitly represent the downstream water demands. The target storages and releases are derived and incorporated into an extended reservoir operation scheme in Section 3.6.1.

3.6. Improving Conceptual Reservoir Operation Models With Remote Sensing

Conceptual reservoir operation models or schemes have been widely used in hydrologic modeling studies to approximate the reservoir operation in the real world (Hanasaki et al., 2006; Shin et al., 2019; Voisin et al., 2013; W. Wang et al., 2017; Zajac et al., 2017). In this study, we use a calibration-free conceptual reservoir operation scheme developed in our previous research to simulate reservoir operation, along with three commonly used conceptual operation schemes. These schemes generally introduce parameters that essentially need to be calibrated from historic operation data for each individual reservoir and, when such data is unavailable, often yield undesirable simulation accuracies. In light of this issue, this study attempts to calibrate these parameters to remotely sensed reservoir storages and reconstructed releases to improve the simulations of ungauged reservoirs for these schemes.

In particular, our previously developed conceptual operation scheme is extended with a storage anomaly based calibration approach, which is tailored to the use of the remotely sensed data that often span periods of only a few years and are often available at intervals of 10–30 days. We introduce this as follows.

3.6.1. Extended Storage Anomaly Based Reservoir Operation Scheme

A conceptual operation scheme originally designed for ungauged reservoirs in our previous research (Dong et al., 2022, hereinafter “D22”) is employed and further extended in this study for reservoirs with remotely sensed reservoir operation data. The release of reservoirs, Q_t , is calculated according to the current water level compared with a few reservoir pool storages:

$$Q_t = \begin{cases} \min\left(Q_{min}, \frac{V_t}{\Delta t}\right) & (V_t \leq V_d) & (6a) \\ \max(Q_{min}, r \cdot U_t) & (V_d < V_t \leq V_c) & (6b) \\ r \cdot U_t + (Q_s - r \cdot U_t) \cdot \left(\frac{V_t - V_c}{V_f - V_c}\right)^k & (V_c < V_t \leq V_f) & (6c) \\ \max\left(Q_s, \frac{V_t - V_f}{\Delta t}\right) & (V_t > V_f) & (6d) \end{cases}$$

where V_t , V_d , V_c , and V_f are the water storages of reservoirs at the model time step t , at the dead storage level, conservation level, and high flood level, respectively (Figure S4 in Supporting Information S1). The conservation level is often higher during the dry season to store water for socioeconomic use (with the corresponding storage denoted V_{cd}) and lower in the wet season to create more space for flood control (with the corresponding storage denoted V_{cw}). In this study, V_d and V_{cd} are collected; V_{cw} can be calibrated, while in this study, it is estimated as the multi-year median reconstructed storage during the month when the reservoir experiences the largest monthly inflow; V_f is assumed the same as V_{cd} , because this is the case for most of China's reservoirs. Q_{min} is the minimum release; U_t is the human water demand at the time step t ; r is a parameter to reflect the storage anomaly; Q_s is the maximum acceptable release; k ($k \leq 1$) is a flood indicator equal to the ratio of Q_s to the inflow.

Our previous studies (Dong et al., 2022, 2023) have demonstrated that the storage anomaly based reservoir operation scheme of Equation 6 is able to represent the multi-purpose reservoir operation. When reservoir storage is below V_d (Equation 6a), the release is set as a minimum value for downstream ecological and emergency socio-economic use, and the water stored in reservoirs is often released through pumping or emergency sluices. When the stored water stands between V_d and V_c (Equation 6b), the reservoir releases water in accordance with the socio-economic needs. When the stored water stands between V_c and V_f (Equation 6c), the reservoir operation attenuates the floods according to the current water storage and the magnitude of incoming floods. At this stage, the reservoir release should not be less than the downstream demands and no more than the maximum release Q_s for downstream security. When the stored water rises above V_f (Equation 6d), all floodgates are open and all water above V_f is released as soon as possible for dam safety.

Note this scheme was originally designed for ungauged reservoirs, where parameters Q_{min} , Q_s , r , and U_t are derived empirically without any need for historic reservoir operation data. Specifically, when in-situ data are not available, Q_{min} and Q_s are set as the 10th and 99th percentiles of non-exceedance probabilities of simulated daily streamflow, respectively. r is derived based on the relative difference between the current storage and the target storage V_{tar} (i.e., the storage anomaly), and r is expressed as $r = 1 + c \cdot (V_t - V_{tar}) / (V_{cd} - V_d)$. Here, V_{tar} is empirically derived from linear interpolation between V_{cd} at the beginning of dry season and V_d at the beginning of the wet season; c is an empirical parameter. More details on parameters c and U_t are provided in Text S2 in Supporting Information S1.

Here, the reconstructed reservoir operation data have the potential to further improve the estimation of these parameters for more accurate representations of reservoir operation. Specifically, the release thresholds Q_{min} and Q_s can be calibrated directly to the reconstructed storages and releases. For the parameter r , a novel parameterization for calibration is proposed with the use of reconstructed reservoir releases, storages, and average operating patterns. The empirical parameter c is calibrated to the reconstructed reservoir storages and releases; and the target releases Q_{tar} are introduced in replace of human water demand U_t to implicitly represent the multi-year averaged downstream water demands at different times of the year. r is then expressed as,

$$r = \frac{Q_{tar}}{U_t} \cdot \left(1 + c \cdot \frac{V_t - V_{tar}}{V_{cd} - V_d}\right) \quad (7)$$

Target releases Q_{tar} and target storages V_{tar} vary at different times of the year and are derived at daily scales in this study. Experiments suggest that daily target releases and target storages corresponding to the 10-day rolling

mean of the multi-year median (multi-year mean) daily reconstructed releases and storages generally perform well for within-year reservoirs (over-year reservoirs), respectively. An advantage of this parameterization is that Q_{tar} and V_{tar} represent the average reservoir operating patterns and can explicitly account for the key features of the reservoir operation rule curves, which can serve to constrain reservoir behaviors in the reservoir operation simulations. This relatively simple model structure reduces the number of parameters and hence the need for long-term, continuous data for parameter calibration. More sophisticated parameterizations can be developed on this basis, if such data are available.

The rationale behind r is to adapt the release to the storage anomalies relative to the target storage—a reservoir operation policy frequently adopted by reservoirs worldwide. While some studies (e.g., Wu & Chen, 2012) also consider the downstream water demand anomalies at different times of the year as part of the release functions, we assume water demand anomalies are a minor factor compared with storage anomalies, which we discuss in detail in Section 5.3.

3.6.2. Existing Reservoir Operation Schemes

Three other conceptual reservoir operation schemes widely used in hydrologic models are also selected for comparison. The first one is selected from Hanasaki et al. (2006, 2008), hereinafter “H08,” and the release of reservoirs in the H08 scheme is,

$$Q_t = \begin{cases} k_y \cdot r_m & (c > \beta) \\ \left(\frac{c}{\beta}\right)^2 \cdot k_y \cdot Q'_t + \left(1 - \frac{c}{\beta}\right)^2 \cdot I_t & (c < \beta) \end{cases} \quad (8)$$

with $c = V_m/I_a$; $k_y = V_{1st}/\alpha V_m$

$$Q'_t = \begin{cases} I_a, & \text{for non-irrigation reservoirs} \\ f(U_t), & \text{for irrigation reservoirs} \end{cases}$$

where V_{1st} is the reservoir storage at the ending month of the wet season during a hydrologic year; I_a is the mean annual total inflow; Q'_t is the provisional release; $f(U_t)$ is a function of downstream water demand, see Hanasaki et al. (2006) for full expressions; α and β are parameters. Hanasaki et al. (2006) did not provide a calibration approach for these parameters but instead suggested empirical default values of $\alpha = 0.85$ and $\beta = 0.5$ for all reservoirs. In this study, we assume these parameters can also be calibrated when reservoir operation data are available.

The second one is selected from the WBM model (Wisser et al., 2010), hereinafter “W10,” and the release of reservoirs in the W10 scheme is,

$$Q_t = \begin{cases} \kappa I_t & (I_t \geq I_a) \\ \lambda I_t + I_a - I_t & (I_t < I_a) \end{cases} \quad (9)$$

where I_a is the mean annual total inflow; I_t is the inflow at the time step t . Similarly, κ and λ are parameters that can be either calibrated to operation records or set empirically as default values of 0.16 and 0.6 (Wisser et al., 2010).

The third one is selected from the LISFLOOD hydrologic model (Zajac et al., 2017), hereinafter “Z17,” and the release of reservoirs in the Z17 scheme can be expressed as,

$$Q_t = \begin{cases} \min\left(Q_{min}, \frac{V_t}{\Delta t}\right) & (V_t \leq V_d) \\ Q_{min} + (Q_{norm} - Q_{min}) \left(\frac{V_t - V_d}{V_c - V_d}\right) & (V_d < V_t \leq V_c) \\ Q_{norm} + \max(I_t - Q_{norm}, Q_{nd} - Q_{norm}) \left(\frac{V_t - V_c}{V_f - V_c}\right) & (V_c < V_t \leq V_f) \\ \max\left(Q_{nd}, \frac{V_t - V_f}{\Delta t}\right) & (V_t > V_f) \end{cases} \quad (10)$$

where Q_{min} , Q_{norm} , and Q_{nd} are the minimum release, normal release, and non-damaging release, respectively. These three parameters can be calibrated if historic reservoir operation records are available. Otherwise, Zajac et al. (2017) suggested empirical default values of the 5th, 30th, and 97th percentiles of the naturalized daily streamflow.

3.7. Experimental Design

To explore the synergistic use of satellite remote sensing and hydrologic modeling in improving the reservoir parameterizations, two series of reservoir operation simulations are set up and performed in this study.

We first perform the release, storage, and hydropower simulations of the two reservoirs with parameters empirically set to their default values (see Sections 3.6.1 and 3.6.2, hereinafter “empirical parameters”) for each reservoir operation scheme. The hydropower output is calculated according to the release and storage, with formulas provided in Text S3 in Supporting Information S1. The simulations both here and in the next paragraph are driven by the daily inflow reconstructed from hydrologic modeling (Section 3.5). Given there is no prior knowledge of the initial water storage, the reconstructed reservoir storage at the beginning of the simulation period is taken as the initial water storage. The subsequent results can serve as a baseline for reservoir operation simulations.

On this basis, we derive the target storage and release for the extended D22 scheme, and calibrate the parameters of all four reservoir operation schemes to the reconstructed reservoir storage and release. Here, the reconstructed storage and releases used for calibration are 10-day averaged values instead of daily values. This is because the daily release and storage are essentially derived from linear interpolation from the 10-day altimetric data and do not really contain useful information but instead may introduce noises within the 10-day interval that are unfavorable to calibration. Therefore, the reconstructed daily release and storage at the 10-day interval (Section 3.5) are averaged over a 10-day period, consistent with the date and interval of the altimetric data. For Jinping I Reservoir, we select 2015–2016 for calibration and 2017–2018 for validation; for Ertan Reservoir, given that the upstream Jinping I Reservoir was put into operation in 2014, we select 2010–2011 for calibration and 2012–2013 for validation. Thus, a total of 73 storage-release data pairs are used for calibration for both reservoirs. The parameters employed for calibration include Q_{min} , Q_s , and c of the extended D22 scheme, α and β of the H08 scheme, κ and λ of the W10 scheme, and Q_{min} , Q_{norm} , and Q_{nd} of the Z17 scheme. For each scheme, 10,000 parameter sets are generated randomly, and the parameter set that gives the maximum average Nash-Sutcliffe Efficiency (NSE) value of the simulated storage and release as compared with the reconstructed 10-day reservoir storage and release is chosen as the best one, hereinafter “calibrated parameters.” A sensitivity test is provided in Text S4 in Supporting Information S1.

Here, the reservoir operation simulations of the Ertan Reservoir are split into two sub-periods, that is, 2010–2013 and 2015–2018, which correspond to the periods before and after the full operation of the upstream Jinping I Reservoir (mid-2014), respectively. Evaluating the simulated storage, release, and hydropower production against the in-situ data during the two sub-periods allows us to specifically investigate the reliability of the four reservoir operation schemes under streamflow variations for long-term scale application.

In addition to the above experiments, to better demonstrate the applicability of the extended D22 to a wider range of reservoirs, additional release and storage simulations are carried out on several other reservoirs as independent test cases. The relevant details and results are provided in Appendix A and in Text S5 in Supporting Information S1.

4. Results

4.1. Calibration and Validation of the CLHMS Model

To reproduce the natural flow regime of the YRB, the CLHMS model without any reservoirs is calibrated (validated) against the daily streamflow of Yajiang station for 2006–2008 (2009–2013) and Ertan station for 2001–2009 (2010–2013). Three parameters of the CLHMS model are calibrated, including the direct runoff parameter d_{cor} , the channel roughness r_o , and the groundwater-surface water exchange coefficient C . For each station, 1,000 parameter sets are sampled using Latin Hypercube sampling, and the parameter sets with the highest NSE are chosen as the optimal set.

Figure 3 presents the calibration and validation results with the percentage bias (PB) and the daily NSE. It shows that the performance of the CLHMS model with no account of reservoirs is satisfactory, with most NSE

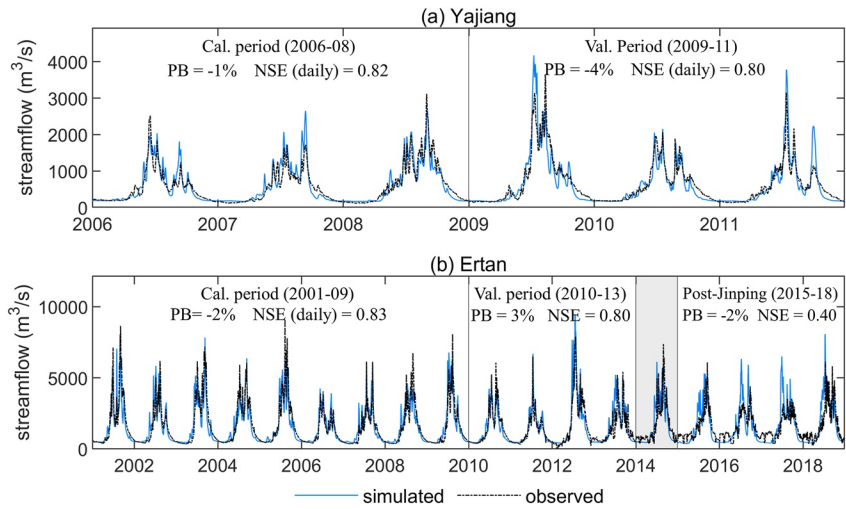


Figure 3. Daily streamflow simulations at (a) Yajiang station and (b) Ertan station, without accounting for reservoirs.

values over 0.80 and RB values less than $\pm 5\%$ during the calibration and validation period. Notably, the NSE in the period of 2015–2018 at the Ertan station (0.4) is considerably lower than that in the calibration period of 2001–2009 (0.83) and that in the validation period of 2010–2013 (0.80). This could be explained by the fact that the Jinping I Reservoir in the YRB was put into operation around 2014, yet the model here is unable to account for the impact of reservoirs on the streamflow during this period.

4.2. Evaluation of Reconstructed Reservoir Storages and Releases

Figure 4 depicts the water area-level relationship, the storage and release of Ertan Reservoir and Jinping I Reservoir reconstructed from satellite altimetry, GSW remote sensing images, and hydrologic modeling. The water level shows a strong linear correlation with the water area for both reservoirs ($R^2 \geq 0.85$). The reconstructed

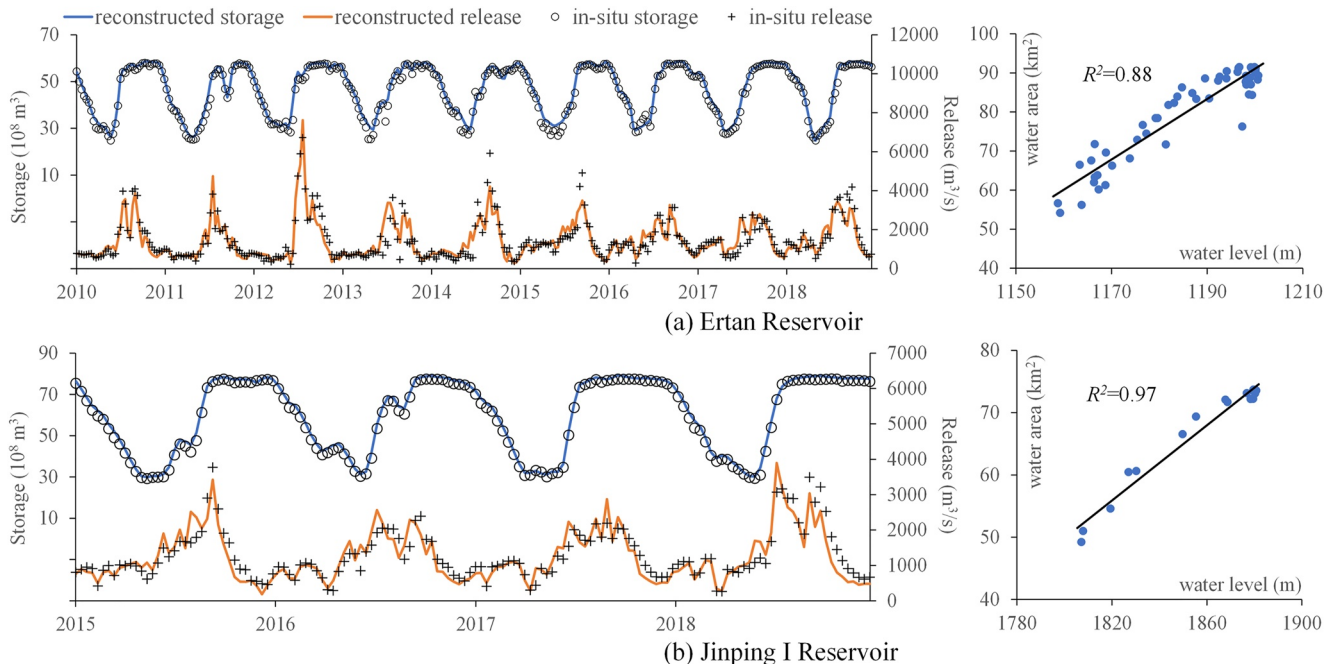


Figure 4. Remotely sensed 10-day storages and reconstructed 10-day releases (left), and the area-level relationship established from the altimetric water level and global surface water water area (right) of (a) Ertan Reservoir and (b) Jinping I Reservoir.

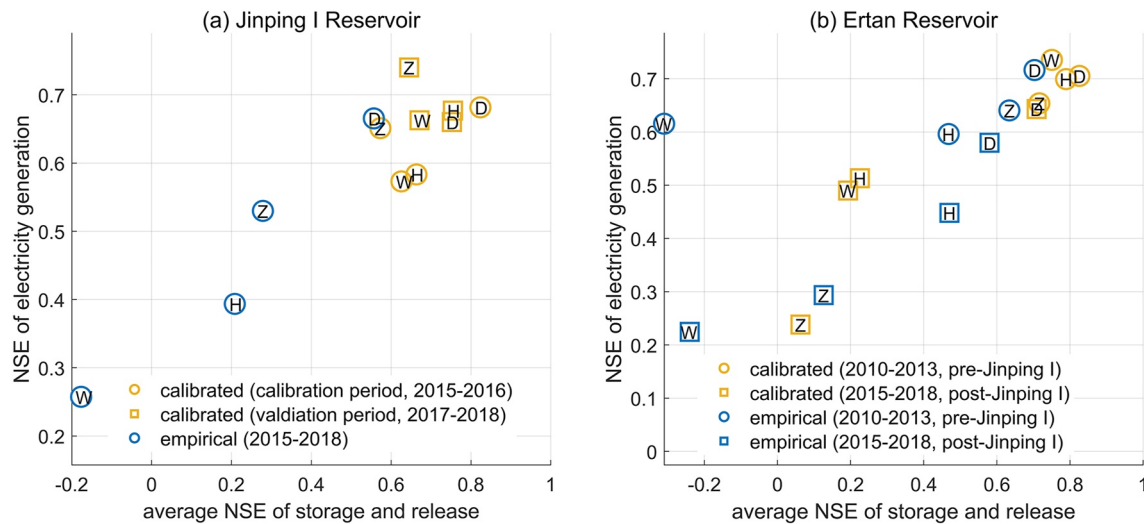


Figure 5. Performance metrics of daily storage, release, and electricity generation simulated by four reservoir operation schemes with parameters calibrated to the reservoir operation data reconstructed from remote sensing (yellow) and parameters empirically set to default values (blue) of (a) Jinping I Reservoir and (b) Ertan Reservoir, as compared with in-situ observations. D – D22; H – H08; W – W10; Z – Z17.

storage (release) matches well with in-situ observations, with 10-day NSE values of 0.97 (0.83) and 0.99 (0.80) for Ertan Reservoir and Jinping I Reservoir, respectively. In terms of the hydrologic extremes, the relative bias of the annual maximum (minimum) 10-day reconstructed release is 0.7% (–11%) for Jinping I Reservoir and –6% (5%) for Ertan Reservoir, respectively. This suggests that our approach in Section 3.5 can reconstruct the reservoir storage and release remotely under hydrologic extremes with a sufficient accuracy at a shorter time scale. The reconstructed reservoir storage and releases are provided in Dong (2022).

To illustrate the effect of reservoir masks and the corresponding reservoir water area on the reconstruction of reservoir water storage, we compare our generated reservoir mask with the GRanD reservoir boundary mask for the two reservoirs (Figure 1b). Results indicate that our generated masks are 69% larger for the Ertan Reservoir and 50% larger for the Jinping I Reservoir than the GRanD polygons. Correspondingly, the relative bias of the reconstructed water storage of both reservoirs reduces from 4% to 5% with the GRSAD water area (i.e., based on the GRanD mask) to around 2% with the derived GSW water area (i.e., based on our DEM-based reservoir mask). More details are provided in Figure S1 in Supporting Information S1.

Another factor that may affect the accuracy of storage and release reconstruction is the precipitation and evaporation on the reservoir water surface. Our results indicate that the mean annual precipitation and evaporation are 1,032 and 975 mm for the Jinping I Reservoir, respectively, and are 1,101 and 1,404 mm for the Ertan Reservoir, respectively. The mean annual net water loss (i.e., evaporation minus precipitation) is thus 19 million m³ (–4.2 million m³) for the Ertan Reservoir (Jinping I Reservoir), accounting for 0.42% (–0.07%) of the mean water storage and 0.04% (–0.01%) of the mean annual inflow. On a daily scale, the net water loss generally accounts for less than 2% of the inflow on all days of the study period, with the mean value around 0.1% for both reservoirs (Figures S2 and S3 in Supporting Information S1). These results indicate that, in our case study, the reservoir precipitation and evaporation are unlikely to have a notable impact on the reservoir water balance at daily to annual scales and during different periods of the year. However, in arid areas where evaporation overwhelms precipitation, the net water loss cannot be neglected.

4.3. Evaluation of Reservoir Operation Simulations Under Streamflow Alterations

4.3.1. Reservoir Simulations With Parameters Empirically Set to Their Default Values

Quantitative metrics of the four sets of simulated reservoir operations with parameters set to their default values in terms of storage, release, and electricity generation are detailed in Figure 5 (blue markers). The model performance results are further illustratively assessed by comparing the daily variations of the simulated storage, release, and electricity generation of the Jinping I Reservoir for 2015–2018 in Figure 6 and those of the Ertan

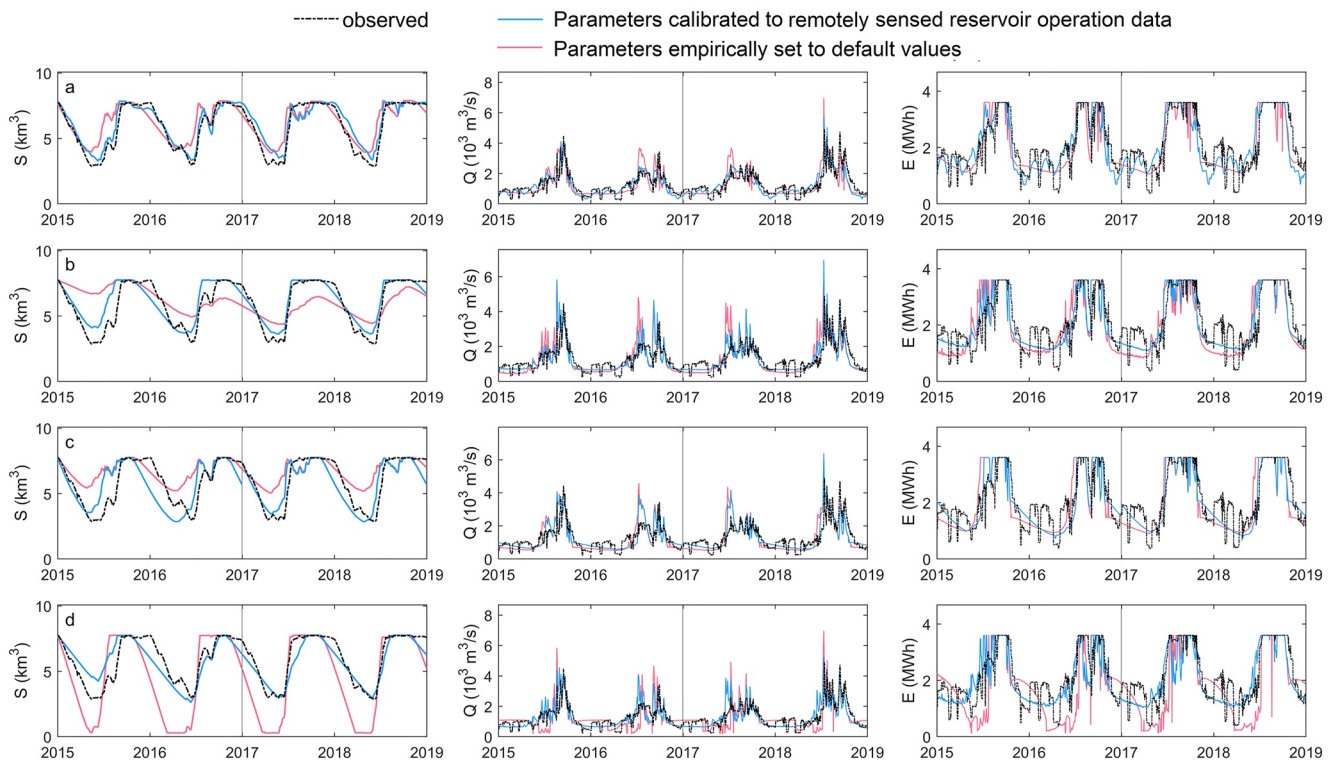


Figure 6. Daily storage (left), release (middle), and electricity production (right) simulations of the Jinping I Reservoir (2015–2018) using (a) D22, (b) H08, (c) Z17, and (d) W10 reservoir operation schemes with the parameters calibrated to the reservoir operation data reconstructed from remote sensing (blue) and the empirical parameters set to their default values (pink), respectively, as compared with in-situ observations.

Reservoir for 2012–2018 with the in-situ operation data in Figure 7, which allows to jointly visualize the reservoir operations with respect to the regional water-energy nexus.

Results indicate that the performances of empirical parameters vary among different schemes. Take the Jinping I Reservoir, for example, the average daily NSE of the reservoir storage and release ranges from -0.18 to 0.58 , and the NSE of the simulated hydropower output ranges from 0.63 to 0.71 . Among all investigated schemes with the empirical parameters, the D22 scheme can comparably better capture the storage variation of Ertan Reservoir during the entire period, with the average daily NSE of simulated release and storage higher than 0.6 over the entire period. Specifically, the simulation accuracy is not significantly impacted by the operation of the upstream Jinping I Reservoir, with the NSE only ~ 0.1 lower after 2014 than before 2014.

4.3.2. Reservoir Simulations With Parameters Calibrated to Reconstructed Operation Data

In this section, we repeat the reservoir operation simulations in Section 4.3.1 but calibrate these parameters against the remotely sensed reservoir operation data in the four investigated schemes. The model performances for the Ertan Reservoir and Jinping I Reservoir are assessed again with the quantitative metrics in Figure 5 (yellow markers) and with the time series plots in Figures 6 and 7. The comparison of the quantitative metric values (yellow markers vs. blue markers in Figure 5) and the daily variations of the simulated storage, release, and electricity generation in the empirical parameters simulations with those in the calibrated parameters simulations (Figures 6 and 7) allows to assess the validity of calibrated parameters in simulations of ungauged reservoirs, and thereby to jointly visualize the benefits of the synergistic use of satellite remote sensing and hydrologic modeling.

In comparison to the simulations with the empirical parameters, all of the schemes with the calibrated parameters show improved simulation accuracies to a varying degree (Figure 5). For example, for Jinping I, the average daily NSE of the reservoir storage and release is 0.58 , 0.27 , -0.18 , and 0.21 for D22, Z17, W10, and H08 schemes with the empirical parameters, and increases to 0.79 , 0.62 , 0.64 , and 0.70 with the calibrated parameters. Similarly, for the Ertan Reservoir, most of the NSE values are higher with the calibrated parameters than with the empirical parameters for the same period (blue markers vs. yellow markers in Figure 5b).

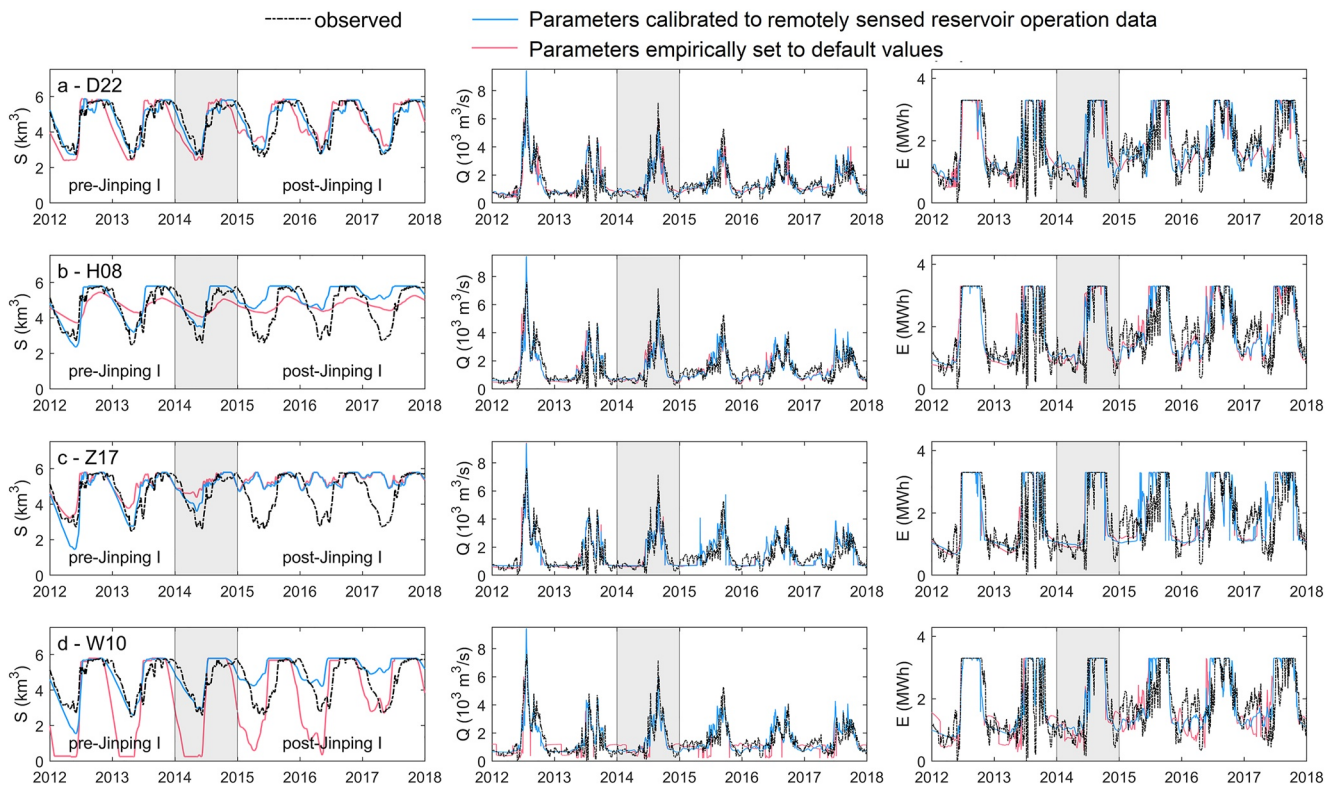


Figure 7. As in Figure 6 but for the Ertan Reservoir (2012–2018). Pre-Jinping I and Post-Jinping I represent the time period before and after the operation of Jinping Reservoir.

A more detailed comparison between different operation schemes is also performed. For Jinping I Reservoir, the accuracy of the operation simulation is rather satisfactory for all conceptual schemes, mostly with a daily NSE of the simulated release and storage larger than 0.6 and a daily NSE of the simulated electricity production larger than 0.55 over the entire period (Figures 5a and 6). For Ertan Reservoir, the daily NSE over the calibration (validation) period is 0.85 (0.80) for our extended D22 scheme, and the NSE in the post-Jinping I period (0.72) is not much lower than that in the pre-Jinping I period (0.82) (Figures 5b and 7). Likewise, the NSE of the simulated hydropower output of the Ertan Reservoir is 0.7 (0.64) in the pre-Jinping I (post-Jinping I) period. This suggests that our extended D22 scheme calibrated to the reconstructed storage and release has the potential to reproduce and predict the release, storage, and hydropower production of the Ertan Reservoir, especially under the changing streamflow regimes of the YRB before and after the operation of Jinping I.

On the other hand, the calibrated H08, W10, and Z17 scheme can capture the storage variation of Ertan Reservoir in 2010–2013 well but fail to reproduce it from 2015 onwards (Figures 5b and 7), in much coincidence with the operation of the upstream Jinping I Reservoir. The average daily NSE of the simulated release and storage fall quickly from ~ 0.7 in the pre-Jinping I period to ~ 0.2 in the post-Jinping I period for the H08, W10, and Z17 schemes (Figure 5b). Similarly, the NSE of the simulated hydropower output decreases from 0.65 to 0.75 in the pre-Jinping I period to 0.4–0.6 in the post-Jinping I period for the H08, W10, and Z17 schemes at daily scales (Figure 5b). This suggests that fixed values of parameters in these three schemes may not be suitable under streamflow regime changes, and they may require re-calibration for a more accurate simulation after 2015.

To further investigate the ability of the extended D22 scheme and other reservoir operation schemes in capturing the hydrologic extremes, the multi-year averaged maximum and minimum 1-day (MAX1/MIN1), 3-day (MAX3/MIN3), 7-day (MAX7/MIN7), 30-day (MAX30/MIN30), and 90-day (MAX90/MIN90) releases simulated by the four schemes are compared with the in-situ release for the two reservoirs. Figure 8 depicts the relative bias of these hydrologic extreme indicators with the four schemes. The relative bias is smaller than 20% for most of the indicators and most of the schemes. For example, the relative biases of the Jinping I Reservoir (Ertan Reservoir) are around 10% (–3%) for high flows and around 0% (5%) for low flows with the extended D22 scheme,

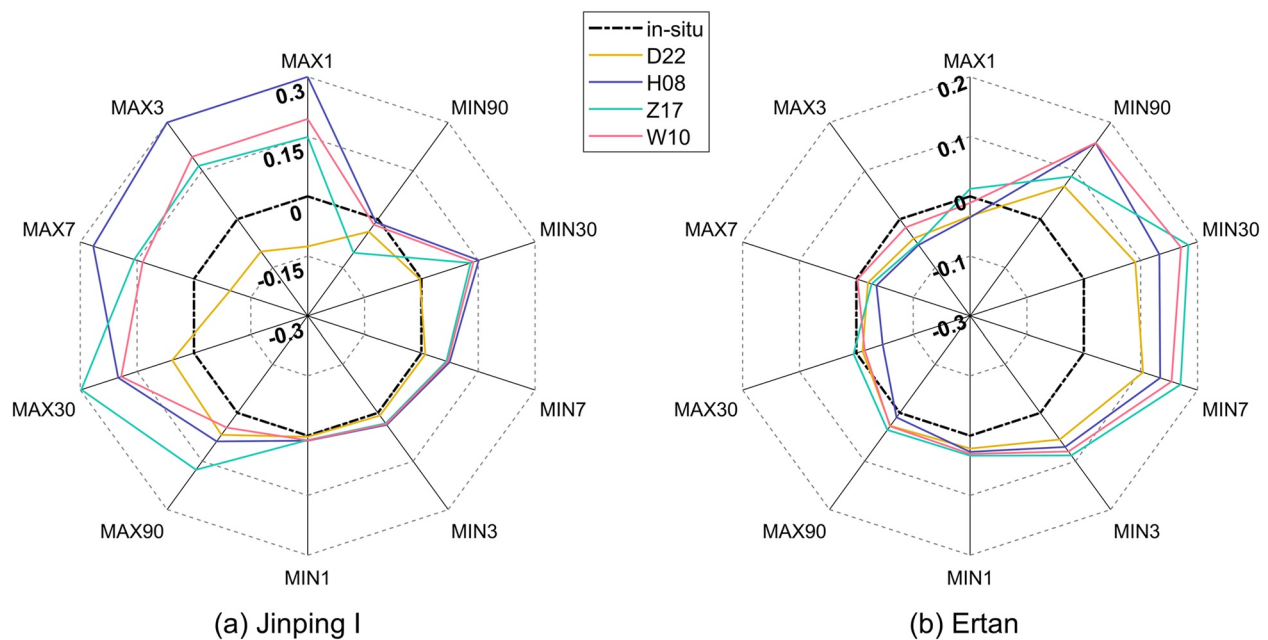


Figure 8. Reservoir release simulations with respect to the hydrologic extremes using the D22, H08, Z17 and W10 schemes with parameters calibrated to reconstructed operation data.

respectively. For the D22 scheme, the lower-than-actual simulated peak flows for the Jinping I Reservoir can be attributed to the underestimation of water storage by $\sim 9\%$ around early September 2016, which leads to a larger flood control storage and the corresponding reservoir release of $\sim 35\%$ smaller than actual. The higher-than-actual simulated low flows for the Ertan Reservoir are attributed to the highly fluctuating in-situ reservoir releases, which sometimes drop to $\sim 200 \text{ m}^3/\text{s}$ (e.g., in mid-2015 and 2016) as compared to the minimum 1-month average release of $\sim 700 \text{ m}^3/\text{s}$. These fluctuations can be hardly represented by the schemes, especially for the other three schemes that do not characterize a storage-release relationship.

These results indicate that the reconstructed reservoir operation releases and storage, despite at a relatively low temporal resolution of 10 days, can contribute to the simulations of high flows and low flows over 1-day to 90-day time scales. When operation data with a higher temporal resolution are available, more accurate model simulations of extreme-flow conditions are expected.

In general, our evaluations in Sections 4.3.1 and 4.3.2 with respect to the calibrated parameters and the empirical parameters suggest that the remote sensing can improve the parameter estimation of the four investigated reservoir operation schemes for ungauged reservoirs, thereby improving the simulations for all selected schemes (Figure 5). It is also noted that, despite the reconstructed reservoir storage and release are at a 10-day frequency, they can be combined with these reservoir schemes to derive fairly accurate high flows and low flows from 1-day to 90-day scales. Comparably, by incorporating time-varying target storages and releases, our extended D22 scheme can better reproduce the storage, release, and electricity production under streamflow alterations, which is further discussed in Section 5.2. On the other hand, the H08, W10, and Z17 schemes can simulate the reservoir operation under the hydrologic stationarity well, but they perform less desirably under a changing inflow regime (blue vs. yellow markers in Figure 5), which could limit their applications over long-term time scales.

4.4. Improvements of Streamflow Simulations Considering Reservoirs

In Section 4.1, the model shows a degraded performance at the Ertan station during 2015–2018, in coincidence with the upstream reservoir operation. To further examine if the lack of reservoir operation is the major cause of the degraded model accuracy in this period, we perform a series of CLHMS simulations by coupling the four reservoir operation schemes with the calibrated parameters and the empirical parameters, respectively. These simulations are then compared with the CLHMS simulation without reservoirs in Section 4.1 for an in-depth analysis.

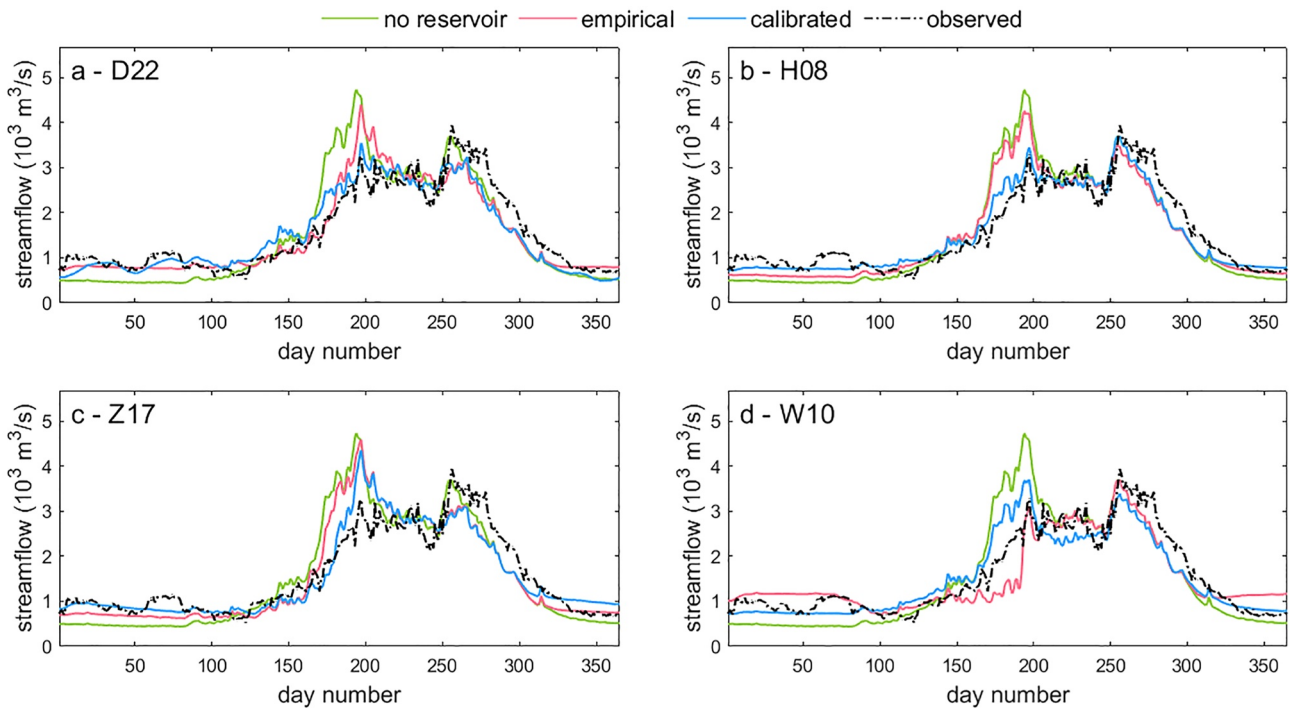


Figure 9. Daily streamflow simulations at the Ertan hydrologic station averaged over the validation period of the coupled land surface-hydrologic model (CLHMS) (2011–2018) before and after integrating reservoirs with (a) D22, (b) H08, (c) Z17, and (d) W10 schemes in the CLHMS model, as compared with in-situ observations.

As indicated in Figure 9, we find that integrating reservoirs in the CLHMS can improve the streamflow simulations during 2015–2018 for all schemes. Among the schemes, our extended D22 scheme with the calibrated parameters makes one of the most significant improvements in the streamflow simulation, as the daily NSE at the Ertan hydrologic station increases from 0.4 to 0.75. For example, the simulated streamflow without (with) reservoirs at the Ertan station is 10.6% (–1.5%) higher than the in-situ streamflow during the wet season and 29.8% (4.9%) lower than the in-situ streamflow during the dry season. The simulated annual maximum 1-day flood also shows improvements, as the relative error decreases from 20% without reservoirs to 9% with reservoirs. The D22 scheme with the empirical parameters can also improve the streamflow simulation but to a lesser degree, with the NSE increasing to 0.65. For other schemes, streamflow and annual maximum flood simulations are also improved for both the calibrated parameters and the empirical parameters.

The above results indicate that the degraded model accuracy in the post-Jinping I period (Section 4.1) can be largely explained by the reservoir impact. The daily NSE can be enhanced to a maximum value of 0.75 after integrating the reservoir operation, which is not much lower than the value of 0.80 in the validation period. In addition to reproducing the dynamics of the two reservoirs well, these validation results at the Ertan station suggest that (a) integrating reservoirs into CLHMS, (b) estimating reservoir surface area and water level from remotely sensed data, and (c) our extended storage anomaly based operation scheme all enable the accurate quantification of the hydrological impact of two ungauged reservoirs in the YRB.

5. Discussion

5.1. Satellite Altimetry as a Promising Tool for Reservoir Impact Assessment and Predictions

As an estimated 2.8 million reservoirs have been constructed globally, recent research efforts in improving the representations of reservoir operation in hydrologic models are flourishing through the development of reservoir operation schemes (Boulange et al., 2021; Zhou et al., 2016). Most of these schemes require detailed reservoir operation rules or historic operation data to determine the optimal structure and parameters (Coerver et al., 2018; Ehsani et al., 2017; Yang et al., 2019). Reservoir operation rules formulated by local water agencies can be used to infer the model structure and parameters directly, which often dictates the desirable reservoir storage and release

under different hydrologic conditions. However, these rules are often not made available to the public, and where these rules are available, it may not be an easy task to have them directly parameterized in hydrologic models for immediate applications. This is because these rules in many cases provide only guidance and constraints with flexibility in meeting the socio-economic demands, and are not always strictly followed by dam operators. In addition, the in-situ operation data are less frequently shared beyond local scales (Wada et al., 2017). These factors limit the accuracy of reservoir operation simulations in ungauged locations.

To address this problem, we systematically investigate and demonstrate the potential of readily available remote sensing for improving the accuracy of reservoir operation simulations and hydrologic predictions. The reservoir operation simulations and downstream hydrologic simulations all experience an enhanced accuracy through calibration against the reservoir operation data reconstructed from the synergistic use of satellite remote sensing and hydrologic modeling (Sections 4.3 and 4.4). While these reconstructed reservoir storages and releases can be embedded with errors and uncertainties, we demonstrate that they can improve model parameterizations and accuracies (Figures 5–7). Although we present a local case study with two reservoirs, our proposed framework assumes in-situ operation data and operation rules are unknown, which has the potential to be applied to predictions in ungauged basins (PUB) (Blöschl et al., 2019). Our framework can also be used to improve current large-scale hydrologic models, as our results demonstrate the possibility of deriving more reasonable parameter values of generic reservoir operation schemes with remote sensing data that are readily available at large scales.

Despite the potential use of satellite altimetry in reservoir operation simulations, we also note that the large-scale applications of satellite altimetry in this aspect may be limited by the large footprint size and wide ground track spacing of the satellites. For example, most of the current studies have focused the use of satellite altimetry on large reservoirs, yet smaller reservoirs have been less studied because of their small surface water extent as compared to the ground track spacing and footprint size of altimetric satellites such as Jason, Sentinel, and Cryosat (Bonnema & Hossain, 2017, 2019; Han et al., 2020). Notably, the ground track spacing and footprint size of recent satellite altimetry projects, such as ICESat and Surface Water and Ocean Topography (SWOT), have dramatically decreased to a magnitude of kilometers and meters, respectively, and have the potential to detect the water level of smaller reservoirs (Cooley et al., 2021). These sensors will hopefully extend the applicability of our framework to small reservoirs in the near future.

5.2. Model Structure as a Key Factor in the Applicability of Reservoir Operation Schemes

In this study, we extended and tailored our previously developed reservoir operation scheme to the use of remotely sensed reservoir operation data in ungauged basins. A major advantage of our extended scheme is its relatively simple model structure as compared with some of the existing conceptual and data-driven operation schemes. The target storages and target releases introduced in the scheme that constrain reservoir behaviors can be directly inferred from remotely sensed operation data (Equation 8). These reduce the number of parameters and hence the need for long-term, continuous data for parameter calibration. In turn, this allows the scheme to be calibrated and validated against remotely sensed reservoir operation data that often span for a short period (e.g., a few years) and are available at a relatively low frequency (e.g., 10–30 days). In our study, the parameter calibration data for both reservoirs consist of a total of 73 data points, yet the calibrated D22 scheme yields relatively satisfactory storage and release simulations during not only the entire period (Figures 6 and 7) but also during extreme hydrologic events (Figure 8). In comparison, data-driven reservoir operation models are often trained against thousands of daily, continuous operation data (Dong et al., 2023; Yang et al., 2019). While it may be possible to train these models using daily values interpolated from remotely sensed operation data, its feasibility and accuracy require future investigation.

Another major advantage of our extended scheme is that it establishes a time-dependent relationship between water storage and release with the introduction of remotely sensed target storages and target releases, making the reservoir operation more consistent with the reality. In reality, reservoir operation is often guided by prescribed reservoir operation rules that can be illustrated by a set of reservoir operation curves in a reservoir operation chart (see Figure S4 in Supporting Information S1) (Han et al., 2020; Y. Zhao et al., 2021). When the current storage rises above an operation rule curve, the release tends to increase, preventing storage overflowing at an inappropriate time, and vice versa. Our extended operation scheme can explicitly depict such a storage-oriented operation policy by adapting the release to the target storages (i.e., average reservoir operation rule curve) at different periods over a year. In contrast, this cannot be automatically achieved by other schemes investigated in our study.

For example, the H08 and W10 schemes in our study are mostly a linear function of the weighted average of the mean annual inflow and the current inflow, with their parameters serving as weights. Adjusting the weights alone according to the reservoir operation data may not be enough to account for the dynamic release-storage relationship consistent with the reservoir operation rules. Even though the Z17 scheme employs storage as part of the release function, the release is essentially determined by a few release thresholds Q_{max} , Q_{nor} , and Q_{min} that do not change over time. While these reservoir operation schemes can exhibit improved performance when calibrated against remotely sensed operation data (blue vs. yellow markers in Figure 5), these disadvantages may mask their potential shortcomings and bring a challenge for these schemes to simulate the reservoir operation with a higher accuracy.

In particular, the above discrepancies in the model structure among reservoir operation schemes can have a more obvious impact on the reservoir operation simulations when the reservoir is subject to inflow regime variations. Notably, the operation of Jinping I Reservoir leads to a 92% increase in the average inflow of Ertan Reservoir during January and March and a 30%-decrease during June and July (see Figure S5 in Supporting Information S1). The monthly Ertan inflow sees a relative variation ranging from -35% to $+117\%$. For four out of the 12 months a year, the 90 percentile monthly inflow during the pre-Jinping period becomes lower than the 10 percentile release during the post-Jinping period. Despite the parameters are well-calibrated pre-Jinping, the post-Jinping release is not well adapted to the significant increase in the inflow during January and March due to the lack of time-dependent coordination between releases and storage in H08, Z17, and W10, as noted earlier. This can be one of the major reasons for the storage overflowing during this period under these schemes.

In this study, we found that the extended D22 scheme performs better than other schemes under the upstream dam construction, which is a common driver of streamflow regime alterations in the context of dam construction worldwide (Richter, 1996). For other drivers of streamflow alterations, such as climate and land use changes, the extended D22 scheme may also have the potential to be applied for adapting to future climate and land-use conditions. However, given the different time scales between the impacts of dam construction and climate/land use changes, there is a need for another set of experiments to test the validity of reservoir operation models under different climate and land-use conditions.

Future work should include parameterizations of jointly operated cascade reservoirs, which currently remain challenging. For example, there can be multiple joint operation modes of a reservoir system, many of which may occur infrequently or last only for a short period, making it difficult to parameterize and achieve satisfactory calibration results of relevant parameters.

5.3. Consideration of Storage Anomalies Versus Water Demand Anomalies in Reservoir Representations

In the extended D22 scheme, the multi-year average socio-economic water demand at different times of the year is implicitly represented by the target release, which is then adjusted with the current water storage anomalies to determine the final release. While adapting releases to storage anomalies is a common operation practice for reservoirs worldwide, the socio-economic water demand may not always stand at the multi-year average value during a specific period of the year (Shah et al., 2019), and the water demand anomalies may also be a consideration when dam operators determine the release during that specific period. However, at ungauged sites (e.g., in this study), the detailed water demand data are often not available and are, consequently, difficult to incorporate in the scheme. To circumvent this challenge, several studies have attempted to infer reservoir water demands from relevant hydrologic variables. For example, Wu and Chen (2012) used the inflow anomalies for the past 30 days as an indicator of the downstream water demand anomalies. Soil moisture anomalies are also a commonly used indicator of irrigation water demand in hydrologic modeling (Yin et al., 2020).

As an attempt to explore the potential of these water demand indicators in improving reservoir operation simulations, we perform two separate experiments by incorporating the inflow anomalies and soil moisture anomalies into the extended D22 scheme, respectively, in a similar manner to storage anomalies (see details in Text S6 in Supporting Information S1). We found that doing so can increase the NSE values of storage and release only by 0.0–0.02 for Ertan, Jinping I and the other 9 reservoirs considered in our study. This suggests that these readily available water demand indicators may not help improve the performance of the extended D22 scheme in ungauged situations. Moreover, through reservoir operation simulations on the other nine reservoirs with irrigation and water supply as a main purpose, we show that the current version of the extended D22 scheme is

generally able to well reconstruct the release and storage variations for most of these reservoirs (see Appendix A and Figure S11 in Supporting Information S1). These results suggest that considering water demand anomalies may not be mandatory for achieving satisfactory reservoir operation simulations. Therefore, the current study excludes the water demand anomalies from the development of the extended D22 scheme. Further improvements may be required in this respect. For example, with process-based water demand modules as in global hydrologic models, explicit water demand volumes instead of water demand indicators can be considered and tested for improved reservoir parameterizations. This will be one of our future research directions.

6. Conclusions

Driven by two open research questions with respect to reservoir representations in hydrologic simulations, we propose a synergistic framework to predict the release, storage, and hydropower production of ungauged reservoirs that combines remotely sensed reservoir operation data with conceptual reservoir operation schemes within a coupled land surface-hydrologic model. A previously developed conceptual operation scheme for ungauged reservoirs (Dong et al., 2022) is specifically extended and tailored to the use of the remotely sensing data that often spans only for a few years and are available at a temporal resolution of 10–30 days. Three other commonly used conceptual reservoir operation schemes are also included in the framework and the subsequent comparative analysis.

By applying the framework to the YRB in China, we found that the reservoir operation simulations of the four schemes and the downstream hydrologic simulations all experience an enhanced accuracy with the synergistic use of satellite altimetry, remote sensing images, and hydrologic modeling. However, hydrologic non-stationarity can degrade the accuracy of reservoir simulation for most of these schemes, which could result in unreliable assessment of water resources and hydropower production. As compared to a few existing conceptual reservoir operation schemes, our extended operation storage anomaly based scheme is more adaptative to hydrologic variations. Hence, it could be more applicable for long-term simulations, possibly because it explicitly establishes a time-variable storage-release relationship as often prescribed in the reservoir operation rules.

As a final remark of this study, our presented framework has implications for hydrologic modeling from regional, continental to global scales, as our results demonstrate the possibility of deriving more reasonable parameter values of generic reservoir operation schemes using remote sensing data that is readily available in many areas globally. With the successful launch of SWOT, the combination of satellite altimetry, hydrologic modeling, and storage anomaly based reservoir representations can serve to better understand the co-evolution of the hydrologic cycle and the reservoir operation at finer spatiotemporal scales.

Appendix A: Additional Evaluation of the Extended D22 Reservoir Operation Scheme

To investigate the applicability of our extended D22 scheme in a wider range of reservoirs, the historic in-situ inflow, release, and storage data of another nine reservoirs, namely, Three Gorges, Danjiangkou, Longyangxia, Fosi, Baishi, Tuanjie, Hongmen, Liujiaxia, and Xiluodu, are collected and used for calibration and evaluation of this reservoir operation scheme. Reservoir information and details on the calibration and validation periods are given in Table S2 in Supporting Information S1. Figure A1 depicts the simulated reservoir releases and storage as compared with the in-situ data.

In general, the daily release and storage simulations are in good agreement with in-situ observations for most of the reservoirs. The daily NSE values of the simulated storage (releases) are higher than 0.8 (0.6) for around 80% of the reservoirs (Figure S11 in Supporting Information S1). Reservoirs with irrigation or water supply as one of the major functions, such as Three Gorges, Tuanjie, Liujiaxia, Danjiangkou and Baishi, mostly show a fairly satisfactory simulation accuracy. Among all, Baishi and Fosi are generally subject to a relatively lower accuracy of release simulations (daily NSE <0.5), and one of the main reasons could be that the inflow and hence release of the two reservoirs are small on average (less than 10 and 1 m³/s, respectively), yet with very strong, sudden fluctuations during the study period. This makes it difficult to precisely capture the release variations on a daily scale. Despite that, the storage simulations of both reservoirs show a satisfactory accuracy of daily NSE >0.80.

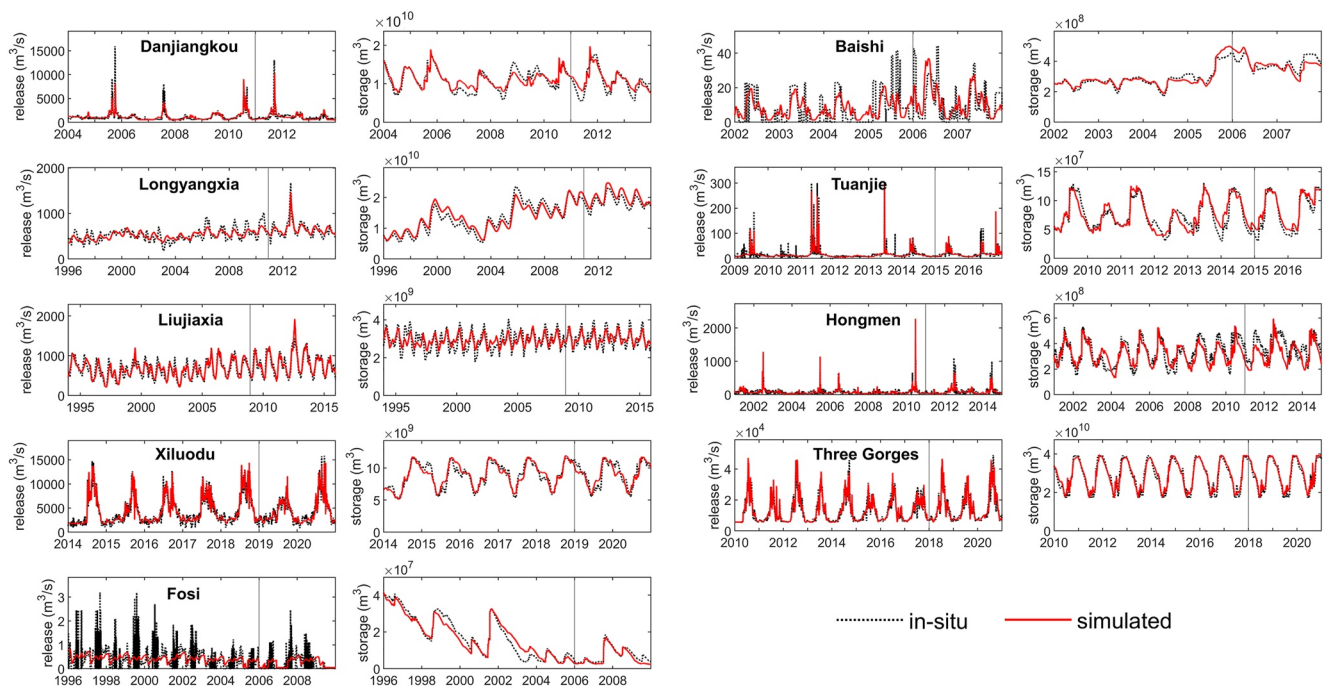


Figure A1. Reservoir release and storage simulations with the extended D22 scheme.

Data Availability Statement

The modeling results and codes of the extended D22 scheme, along with in-situ and satellite-based reservoir operation data and other supporting information, are provided by Dong (2022), available at <https://doi.org/10.5281/zenodo.7190469>. The JRC global water surface data are provided by JRC (2016), available at <https://global-surface-water.appspot.com/download>. The data set of GRSAD global reservoir surface area is provided by Gao and Zhao (2019), available at <https://doi.org/10.18738/T8/DF80WG>. The Jason-2/3 altimetry data are provided by AVISO CNES Data Center (2018), available at the left column of <https://aviso-data-center.cnes.fr/> (registration required).

References

Arheimer, B., Donnelly, C., & Lindström, G. (2017). Regulation of snow-fed rivers affects flow regimes more than climate change. *Nature Communications*, 8, 1–9. <https://doi.org/10.1038/s41467-017-00092-8>

AVISO CNES Data Center. (2018). Jason-2/3 Geophysical Data Records (GDR) [Dataset]. AVISO CNES Data Center. <https://aviso-data-center.cnes.fr/>

Avisse, N., Tilmant, A., Müller, M. F., & Zhang, H. (2017). Monitoring small reservoirs' storage with satellite remote sensing in inaccessible areas. *Hydrology and Earth System Sciences*, 21(12), 6445–6459. <https://doi.org/10.5194/hess-21-6445-2017>

Blöschl, G., Bierkens, M. F., Chambel, A., Cudennec, C., Destouni, G., Fiori, A., et al. (2019). Twenty-three unsolved problems in hydrology (UPH)—A community perspective. *Hydrological Sciences Journal*, 64(10), 1141–1158.

Bonnema, M., & Hossain, F. (2017). Inferring reservoir operating patterns across the Mekong Basin using only space observations. *Water Resources Research*, 53(5), 3791–3810. <https://doi.org/10.1002/2016wr019978>

Bonnema, M., & Hossain, F. (2019). Assessing the potential of the surface water and ocean topography mission for reservoir monitoring in the Mekong River Basin. *Water Resources Research*, 55(1), 444–461. <https://doi.org/10.1029/2018wr023743>

Boulangé, J., Hanasaki, N., Yamazaki, D., & Pokhrel, Y. (2021). Role of dams in reducing global flood exposure under climate change. *Nature Communications*, 12, 1–7. <https://doi.org/10.1038/s41467-020-20704-0>

Busker, T., de Roo, A., Gelati, E., Schwatke, C., Adamovic, M., Bisselink, B., et al. (2019). A global lake and reservoir volume analysis using a surface water dataset and satellite altimetry. *Hydrology and Earth System Sciences*, 23(2), 669–690. <https://doi.org/10.5194/hess-23-669-2019>

CECL. (2003). Feasibility report of Jinping I reservoir. Tech. rep. Chengdu Engineering Corporation Limited.

Chen, T., Song, C., Luo, S., Ke, L., Liu, K., & Zhu, J. (2022). Monitoring global reservoirs using ICESat-2: Assessment on spatial coverage and application potential. *Journal of Hydrology*, 604, 127257. <https://doi.org/10.1016/j.jhydrol.2021.127257>

Chen, T., Song, C., Zhan, P., Yao, J., Li, Y., & Zhu, J. (2022). Remote sensing estimation of the flood storage capacity of basin-scale lakes and reservoirs at high spatial and temporal resolutions. *Science of the Total Environment*, 807, 150772. <https://doi.org/10.1016/j.scitotenv.2021.150772>

Coerver, H. M., Rutten, M. M., & Van De Giesen, N. C. (2018). Deduction of reservoir operating rules for application in global hydrological models. *Hydrology and Earth System Sciences*, 22(1), 831–851. <https://doi.org/10.5194/hess-22-831-2018>

Acknowledgments

The authors thank the editor, two anonymous reviewers, and the third reviewer, Dr. Xudong Zhou, for their in-depth reviews and comments. This work was financially supported by the National Key Research and Development Project of China (Grant 2021YFC3000202), the Belt and Road Special Foundation of the State Key Laboratory of Hydrology-Water Resources and Hydraulic Engineering (2021490311, 2020490711), the German Research Foundation through funding of the AccHydro project (DFG Grant KU, 2090/11-1), and the German Federal Ministry of Science of Education through funding of the MitRiskFlood project (BMBF Grant 01LP2005A). Open Access funding enabled and organized by Projekt DEAL.

- Cooley, S. W., Ryan, J. C., & Smith, L. C. (2021). Human alteration of global surface water storage variability. *Nature*, 591(7848), 78–81. <https://doi.org/10.1038/s41586-021-03262-3>
- Créteaux, J.-F., Biancamaria, S., Arsen, A., Bergé-Nguyen, M., & Becker, M. (2015). Global surveys of reservoirs and lakes from satellites and regional application to the Syrdarya river basin. *Environmental Research Letters*, 10(1), 015002. <https://doi.org/10.1088/1748-9326/10/1/015002>
- Dang, T. D., Chowdhury, A., & Galelli, S. (2020). On the representation of water reservoir storage and operations in large-scale hydrological models: Implications on model parameterization and climate change impact assessments. *Hydrology and Earth System Sciences*, 24(1), 397–416. <https://doi.org/10.5194/hess-24-397-2020>
- Dong, N. (2022). Reservoir operation data and codes [Dataset]. Zenodo. <https://doi.org/10.5281/zenodo.7190469>
- Dong, N., Guan, W., Cao, J., Zou, Y., Yang, M., Wei, J., et al. (2023). A hybrid hydrologic modelling framework with data-driven and conceptual reservoir operation schemes for reservoir impact assessment and predictions. *Journal of Hydrology*, 619, 129246. <https://doi.org/10.1016/j.jhydrol.2023.129246>
- Dong, N., Wei, J., Yang, M., Yan, D., Yang, C., Gao, H., et al. (2022). Model estimates of China's terrestrial water storage variations due to reservoir operation. *Water Resources Research*, 58(6), e2021WR031787. <https://doi.org/10.1029/2021WR031787>
- Du, T. L., Lee, H., Bui, D. D., Graham, L. P., Darby, S. D., Pechlivanidis, I. G., et al. (2022). Streamflow prediction in highly regulated, transboundary watersheds using multi-basin modeling and remote sensing imagery. *Water Resources Research*, 58(3), e2021WR031191. <https://doi.org/10.1029/2021WR031191>
- Ehsani, N., Fekete, B. M., Vörösmarty, C. J., & Tessler, Z. D. (2016). A neural network based general reservoir operation scheme. *Stochastic Environmental Research and Risk Assessment*, 30(4), 1151–1166. <https://doi.org/10.1007/s00477-015-1147-9>
- Ehsani, N., Vörösmarty, C. J., Fekete, B. M., & Stakhiv, E. Z. (2017). Reservoir operations under climate change: Storage capacity options to mitigate risk. *Journal of Hydrology*, 555, 435–446. <https://doi.org/10.1016/j.jhydrol.2017.09.008>
- Eldardiry, H., & Hossain, F. (2019). Understanding reservoir operating rules in the transboundary Nile River Basin using macroscale hydrologic modeling with satellite measurements. *Journal of Hydrometeorology*, 20(11), 2253–2269. <https://doi.org/10.1175/jhm-d-19-0058.1>
- Fan, C., Song, C., Liu, K., Ke, L., Xue, B., Chen, T., & Cheng, J. (2020). Century-scale reconstruction of water storage changes of the largest Lake in the Inner Mongolia plateau using a machine learning approach. *Water Resources Research*, 57(2), e2020WR028831. <https://doi.org/10.1029/2020wr028831>
- Fleischmann, A., Bréda, J., Passaia, O., Wongchuig, S., Fan, F., Paiva, R., et al. (2021). Regional scale hydrodynamic modeling of the river-floodplain-reservoir continuum. *Journal of Hydrology*, 596, 126114. <https://doi.org/10.1016/j.jhydrol.2021.126114>
- Gain, A. K., Giupponi, C., & Wada, Y. (2016). Measuring global water security towards sustainable development goals. *Environmental Research Letters*, 11(12), 124015. <https://doi.org/10.1088/1748-9326/11/12/124015>
- Gao, H. (2015). Satellite remote sensing of large lakes and reservoirs: From elevation and area to storage. *Wiley Interdisciplinary Reviews: Water*, 2(2), 147–157. <https://doi.org/10.1002/wat2.1065>
- Gao, H., & Zhao, G. (2019). Global Reservoir Surface Area Dataset (GRSAD) [Dataset]. Texas Data Repository. <https://doi.org/10.18738/T8/DF80WG>
- Gao, H., Birkett, C., & Lettenmaier, D. P. (2012). Global monitoring of large reservoir storage from satellite remote sensing. *Water Resources Research*, 48(9), W09504. <https://doi.org/10.1029/2012WR012063>
- Giuliani, M., Anghileri, D., Castelletti, A., Vu, P. N., & Soncini-Sessa, R. (2016). Large storage operations under climate change: Expanding uncertainties and evolving tradeoffs. *Environmental Research Letters*, 11(3), 035009. <https://doi.org/10.1088/1748-9326/11/3/035009>
- Grill, G., Ouellet Dallaire, C., Fluet Chouinard, E., Sindorf, N., & Lehner, B. (2014). Development of new indicators to evaluate river fragmentation and flow regulation at large scales: A case study for the Mekong River Basin. *Ecological Indicators*, 45, 148–159. <https://doi.org/10.1016/j.ecolind.2014.03.026>
- Gu, H., Yu, Z., Yang, C., & Ju, Q. (2018). Projected changes in hydrological extremes in the Yangtze River basin with an ensemble of regional climate simulations. *Water*, 10(9), 1279. <https://doi.org/10.3390/W10091279>
- Han, Z., Long, D., Huang, Q., Li, X., Zhao, F., & Wang, J. (2020). Improving reservoir outflow estimation for ungauged basins using satellite observations and a hydrological model. *Water Resources Research*, 56(9), e2020WR027590. <https://doi.org/10.1029/2020wr027590>
- Hanasaki, N., Kanae, S., & Oki, T. (2006). A reservoir operation scheme for global river routing models. *Journal of Hydrology*, 327(1–2), 22–41. <https://doi.org/10.1016/j.jhydrol.2005.11.011>
- Hanasaki, N., Kanae, S., Oki, T., Masuda, K., Motoya, K., Shirakawa, N., et al. (2008). An integrated model for the assessment of global water resources—Part 1: Model description and input meteorological forcing. *Hydrology and Earth System Sciences*, 12(4), 1007–1025. <https://doi.org/10.5194/hess-12-1007-2008>
- Hanasaki, N., Yoshikawa, S., Pokhrel, Y., & Kanae, S. (2018). A global hydrological simulation to specify the sources of water used by humans. *Hydrology and Earth System Sciences*, 22(1), 789–817. <https://doi.org/10.5194/hess-22-789-2018>
- Hoang, L. P., van Vliet, M. T., Kummerow, M., Lauri, H., Koponen, J., Supit, I., et al. (2019). The Mekong's future flows under multiple drivers: How climate change, hydropower developments and irrigation expansions drive hydrological changes. *Science of the Total Environment*, 649, 601–609. <https://doi.org/10.1016/j.scitotenv.2018.08.160>
- Huang, Q., Long, D., Du, M., Han, Z., & Han, P. (2020). Daily continuous river discharge estimation for ungauged basins using a hydrologic model calibrated by satellite altimetry: Implications for the SWOT mission. *Water Resources Research*, e2020WR027309. <https://doi.org/10.1029/2020WR027309>
- Huang, Q., Long, D., Du, M., Zeng, C., Li, X., Hou, A., & Hong, Y. (2018). An improved approach to monitoring Brahmaputra River water levels using retracked altimetry data. *Remote Sensing of Environment*, 211, 112–128–128. <https://doi.org/10.1016/j.rse.2018.04.018>
- JRC. (2016). Global Surface Water [Dataset]. Joint Research Center (JRC). <https://global-surface-water.appspot.com/download>
- Kalnay, E., Kanamitsu, M., Kistler, R., Collins, W., Deaven, D., Gandin, L., et al. (1996). The NCEP/NCAR 40-year reanalysis project. *Bulletin of the American Meteorological Society*, 77(3), 437–471. [https://doi.org/10.1175/1520-0477\(1996\)077<0437:tnyrp>2.0.co;2](https://doi.org/10.1175/1520-0477(1996)077<0437:tnyrp>2.0.co;2)
- Lehner, B., Liermann, C. R., Revenga, C., Vörösmarty, C., Fekete, B., Crouzet, P., et al. (2011). High-resolution mapping of the world's reservoirs and dams for sustainable river-flow management. *Frontiers in Ecology and the Environment*, 9(9), 494–502. <https://doi.org/10.1890/100125>
- Li, X., Long, D., Huang, Q., Han, P., Zhao, F., & Wada, Y. (2019). High-temporal-resolution water level and storage change data sets for lakes on the Tibetan Plateau during 2000–2017 using multiple altimetric missions and Landsat-derived lake shoreline positions. *Earth System Science Data*, 11(4), 1603–1627. <https://doi.org/10.5194/essd-11-1603-2019>
- Liu, J., Yang, H., Gosling, S. N., Kummerow, M., Flörke, M., Pfister, S., et al. (2017). Water scarcity assessments in the past, present, and future. *Earth's Future*, 5(6), 545–559. <https://doi.org/10.1002/2016ef000518>
- Loveland, T. R., Reed, B. C., Brown, J. F., Ohlen, D. O., Zhu, Z., Yang, L., & Merchant, J. W. (2000). Development of a global land cover characteristics database and IGBP DISCover from 1 km AVHRR data. *International Journal of Remote Sensing*, 21(6–7), 1303–1330. <https://doi.org/10.1080/014311600210191>

- Lu, W., Lei, H., Yang, D., Tang, L., & Miao, Q. (2018). Quantifying the impacts of small dam construction on hydrological alterations in the Jiulong river basin of Southeast China. *Journal of Hydrology*, 567, 382–392. <https://doi.org/10.1016/j.jhydrol.2018.10.034>
- McMahon, T. A., Peel, M. C., Lowe, L., Srikanthan, R., & McVicar, T. R. (2013). Estimating actual, potential, reference crop and pan evaporation using standard meteorological data: A pragmatic synthesis. *Hydrology and Earth System Sciences*, 17(4), 1331–1363. <https://doi.org/10.5194/hess-17-1331-2013>
- Nachtergaele, F., van Velthuizen, H., Verelst, L., Batjes, N. H., Dijkshoorn, K., van Engelen, V. W., et al. (2010). The harmonized world soil database. *Proceedings of the 19th world congress of soil science* (pp. 34–37). Soil Solutions for a Changing World.
- O'Neill, B. C., Oppenheimer, M., Warren, R., Hallegatte, S., Kopp, R. E., Pörtner, H. O., et al. (2017). IPCC reasons for concern regarding climate change risks. *Nature Climate Change*, 7(1), 28–37. <https://doi.org/10.1038/nclimate3179>
- Pekel, J. F., Cottam, A., Gorelick, N., & Belward, A. S. (2016). High-resolution mapping of global surface water and its long-term changes. *Nature*, 540(7633), 418–422. <https://doi.org/10.1038/nature20584>
- Penman, H. L. (1948). Natural evaporation from open water, bare soil and grass. *Proceedings of the Royal Society of London. Series A*, 193(1032), 120–145. <https://doi.org/10.1098/rspa.1948.0037>
- Richter, B. D., Baumgartner, J. V., Powell, J., & Braun, D. P. (1996). A method for assessing hydrologic alteration within ecosystems. *Conservation Biology*, 10(4), 1163–1174. <https://doi.org/10.1046/j.1523-1739.1996.10041163.x>
- Ruijsch, J., Verstegen, J. A., Sutanudjaja, E. H., & Karssenberg, D. (2021). Systemic change in the Rhine-Meuse basin: Quantifying and explaining parameters trends in the PCR-GLOBWB global hydrological model. *Advances in Water Resources*, 155, 104. <https://doi.org/10.1016/j.advwatres.2021.104013>
- Shah, H. L., Zhou, T., Sun, N., Huang, M., & Mishra, V. (2019). Roles of irrigation and reservoir operations in modulating terrestrial water and energy budgets in the Indian Subcontinental River basins. *Journal of Geophysical Research: Atmospheres*, 124(23), 12915–12936. <https://doi.org/10.1029/2019jd031059>
- Shen, Y., Liu, D., Jiang, L., Nielsen, K., Yin, J., Liu, J., & Bauer-Gottwein, P. (2022). High-resolution water level and storage variation datasets for 338 reservoirs in China during 2010–2021. *Earth System Science Data*, 14(12), 5671–5694. <https://doi.org/10.5194/essd-14-5671-2022>
- Shin, S., Pokhrel, Y., & Miguez-Macho, G. (2019). High-resolution modeling of reservoir release and storage dynamics at the continental scale. *Water Resources Research*, 55(1), 787–810. <https://doi.org/10.1029/2018wr023025>
- Solander, K. C., Reager, J. T., Thomas, B. F., David, C. H., & Famiglietti, J. S. (2016). Simulating human water regulation: The development of an optimal complexity, climate-adaptive reservoir management model for an LSM. *Journal of Hydrometeorology*, 17(3), 725–744. <https://doi.org/10.1175/jhm-d-15-0056.1>
- Tian, W., Liu, X., Wang, K., Bai, P., & Liu, C. (2021). Estimation of reservoir evaporation losses for China. *Journal of Hydrology*, 596, 126142. <https://doi.org/10.1016/j.jhydrol.2021.126142>
- Turner, S. W., Doering, K., & Voisin, N. (2020). Data-driven reservoir simulation in a large-scale hydrological and water resource model. *Water Resources Research*, 56(10), e2020WR027902. <https://doi.org/10.1029/2020wr027902>
- Veldkamp, T. I. E., Zhao, F., Ward, P. J., de Moel, H., Aerts, J. C., Schmied, H. M., et al. (2018). Human impact parameterizations in global hydrological models improve estimates of monthly discharges and hydrological extremes: A multi-model validation study. *Environmental Research Letters*, 13(5), 055008. <https://doi.org/10.1088/1748-9326/aab96f>
- Voisin, N., Li, H., Ward, D., Huang, M., Wigmosta, M., & Leung, L. R. (2013). On an improved sub-regional water resources management representation for integration into earth system models. *Hydrology and Earth System Sciences*, 17(9), 3605–3622. <https://doi.org/10.5194/hess-17-3605-2013>
- Vu, D. T., Dang, T. D., Galelli, S., & Hossain, F. (2022). Satellite observations reveal 13 years of reservoir filling strategies, operating rules, and hydrological alterations in the Upper Mekong River basin. *Hydrology and Earth System Sciences*, 26(9), 2345–2364. <https://doi.org/10.5194/hess-26-2345-2022>
- Wada, Y., Bierkens, M. F., Roo, A. d., Dirmeyer, P. A., Famiglietti, J. S., Hanasaki, N., et al. (2017). Human–water interface in hydrological modelling: Current status and future directions. *Hydrology and Earth System Sciences*, 21(8), 4169–4193. <https://doi.org/10.5194/hess-21-4169-2017>
- Wada, Y., de Graaf, I. E., & van Beek, L. P. (2016). High-resolution modeling of human and climate impacts on global water resources. *Journal of Advances in Modeling Earth Systems*, 8(2), 735–763. <https://doi.org/10.1002/2015ms000618>
- Wagner, S., Fersch, B., Yuan, F., Yu, Z., & Kunstmann, H. (2016). Fully coupled atmospheric-hydrological modeling at regional and long-term scales: Development, application, and analysis of WRF-HMS. *Water Resources Research*, 52(4), 3187–3211. <https://doi.org/10.1002/2015WR018185>
- Wan, W., Zhao, J., Popat, E., Herbert, C., & Döll, P. (2021). Analyzing the impact of streamflow drought on hydroelectricity production: A global-scale study. *Water Resources Research*, 57, e2020WR028087. <https://doi.org/10.1029/2020WR028087>
- Wang, J., Walter, B. A., Yao, F., Song, C., Ding, M., Maroof, A. S., et al. (2022). GeoDAR: Georeferenced global dams and reservoirs dataset for bridging attributes and geolocations. *Earth System Science Data*, 14(4), 1869–1899. <https://doi.org/10.5194/essd-14-1869-2022>
- Wang, W., Lu, H., Ruby Leung, L., Li, H. Y., Zhao, J., Tian, F., et al. (2017). Dam construction in Lancang-Mekong River Basin could mitigate future flood risk from warming-induced intensified rainfall. *Geophysical Research Letters*, 44(20), 10378–10386. <https://doi.org/10.1002/2017GL075037>
- Wang, Y., Li, J., Zhang, T., & Wang, B. (2019). Changes in drought propagation under the regulation of reservoirs and water diversion. *Theoretical and Applied Climatology*, 138(1–2), 701–711. <https://doi.org/10.1007/s00704-019-02839-3>
- Wei, J., Dong, N., Fersch, B., Arnault, J., Wagner, S., Laux, P., et al. (2021). Role of reservoir regulation and groundwater feedback in a simulated ground-soil-vegetation continuum: A long-term regional scale analysis. *Hydrological Processes*, 35(8), e14341. <https://doi.org/10.1002/hyp.14341>
- Wisser, D., Fekete, B. M., Vörösmarty, C. J., & Schumann, A. H. (2010). Reconstructing 20th century global hydrography: A contribution to the Global Terrestrial Network-Hydrology (GTN-H). *Hydrology and Earth System Sciences*, 14(1), 1–24. <https://doi.org/10.5194/hess-14-1-2010>
- Wu, J., & Gao, X. (2013). A gridded daily observation dataset over China region and comparison with the other datasets. *Chinese Journal of Geophysics*, 56(4), 1102–1111.
- Wu, Y., & Chen, J. (2012). An operation-based scheme for a multiyear and multipurpose reservoir to enhance macroscale hydrologic models. *Journal of Hydrometeorology*, 13(13), 270–283. <https://doi.org/10.1175/jhm-d-10-05028.1>
- Xu, R., Zeng, Z., Pan, M., Ziegler, A. D., Holden, J., Spracklen, D. V., et al. (2023). A global-scale framework for hydropower development incorporating strict environmental constraints. *Nature Water*, 1(1), 113–122. <https://doi.org/10.1038/s44221-022-00004-1>
- Yang, S., Yang, D., Chen, J., & Zhao, B. (2019). Real-time reservoir operation using recurrent neural networks and inflow forecast from a distributed hydrological model. *Journal of Hydrology*, 579, 124229. <https://doi.org/10.1016/j.jhydrol.2019.124229>

- Yassin, F., Razavi, S., Elshamy, M., Davison, B., Sapriza-Azuri, G., & Wheatler, H. (2019). Representation and improved parameterization of reservoir operation in hydrological and land-surface models. *Hydrology and Earth System Sciences*, 23(9), 3735–3764. <https://doi.org/10.5194/hess-23-3735-2019>
- Yin, Z., Wang, X., Ottlé, C., Zhou, F., Guimberteau, M., Polcher, J., et al. (2020). Improvement of the irrigation scheme in the ORCHIDEE land surface model and impacts of irrigation on regional water budgets over China. *Journal of Advances in Modeling Earth Systems*, 12(4), e2019MS001770. <https://doi.org/10.1029/2019ms001770>
- Yoon, Y., & Beighley, E. (2015). Simulating streamflow on regulated rivers using characteristic reservoir storage patterns derived from synthetic remote sensing data. *Hydrological Processes*, 29(8), 2014–2026. <https://doi.org/10.1002/hyp.10342>
- Yoon, Y., Beighley, E., Lee, H., Pavelsky, T., & Allen, G. (2015). Estimating flood discharges in reservoir-regulated river basins by integrating synthetic SWOT satellite observations and hydrologic modeling. *Journal of Hydrologic Engineering*, 21(4), 05015030. [https://doi.org/10.1061/\(asce\)he.1943-5584.0001320](https://doi.org/10.1061/(asce)he.1943-5584.0001320)
- Yu, Z., Lakhtakia, M. N., Yarnal, B., White, R. A., Miller, D. A., Frakes, B., et al. (1999). Simulating the river-basin response to atmospheric forcing by linking a mesoscale meteorological model and hydrologic model system. *Journal of Hydrology*, 218(1–2), 72–91. [https://doi.org/10.1016/S0022-1694\(99\)00022-0](https://doi.org/10.1016/S0022-1694(99)00022-0)
- Yu, Z., Pollard, D., & Cheng, L. (2006). On continental-scale hydrologic simulations with a coupled hydrologic model. *Journal of Hydrology*, 331(1–2), 110–124. <https://doi.org/10.1016/j.jhydrol.2006.05.021>
- Zajac, Z., Revilla-Romero, B., Salamon, P., Burek, P., Hirpa, F. A., & Beck, H. (2017). The impact of lake and reservoir parameterization on global streamflow simulation. *Journal of Hydrology*, 548, 552–568. <https://doi.org/10.1016/j.jhydrol.2017.03.022>
- Zhao, G., & Gao, H. (2019). Estimating reservoir evaporation losses for the United States: Fusing remote sensing and modeling approaches. *Remote Sensing of Environment*, 226, 109–124. <https://doi.org/10.1016/j.rse.2019.03.015>
- Zhao, G., Gao, H., Naz, B. S., Kao, S. C., & Voisin, N. (2016). Integrating a reservoir regulation scheme into a spatially distributed hydrological model. *Advances in Water Resources*, 98, 16–31. <https://doi.org/10.1016/j.advwatres.2016.10.014>
- Zhao, Y., Dong, N., Li, Z., Zhang, W., Yang, M., & Wang, H. (2021). Future precipitation, hydrology and hydropower generation in the Yalong River Basin: Projections and analysis. *Journal of Hydrology*, 602, 126738. <https://doi.org/10.1016/j.jhydrol.2021.126738>
- Zhong, R., Zhao, T., & Chen, X. (2020). Hydrological model calibration for dammed basins using satellite altimetry information. *Water Resources Research*, 56(8), e2020WR027442. <https://doi.org/10.1029/2020wr027442>
- Zhong, W., Guo, J., Chen, L., Zhou, J., Zhang, J., & Wang, D. (2020). Future hydropower generation prediction of large-scale reservoirs in the upper Yangtze River basin under climate change. *Journal of Hydrology*, 588, 125013. <https://doi.org/10.1016/j.jhydrol.2020.125013>
- Zhou, T., Nijssen, B., Gao, H., & Lettenmaier, D. P. (2016). The contribution of reservoirs to global land surface water storage variations. *Journal of Hydrometeorology*, 17(1), 309–325. <https://doi.org/10.1175/jhm-d-15-0002.1>

References From the Supporting Information

- Neitsch, S. L., Arnold, J. G., Kiniry, J. R., & Williams, J. R. (2011). *Soil and water assessment tool theoretical documentation version 2009, Tech. rep.* Texas Water Resources Institute.